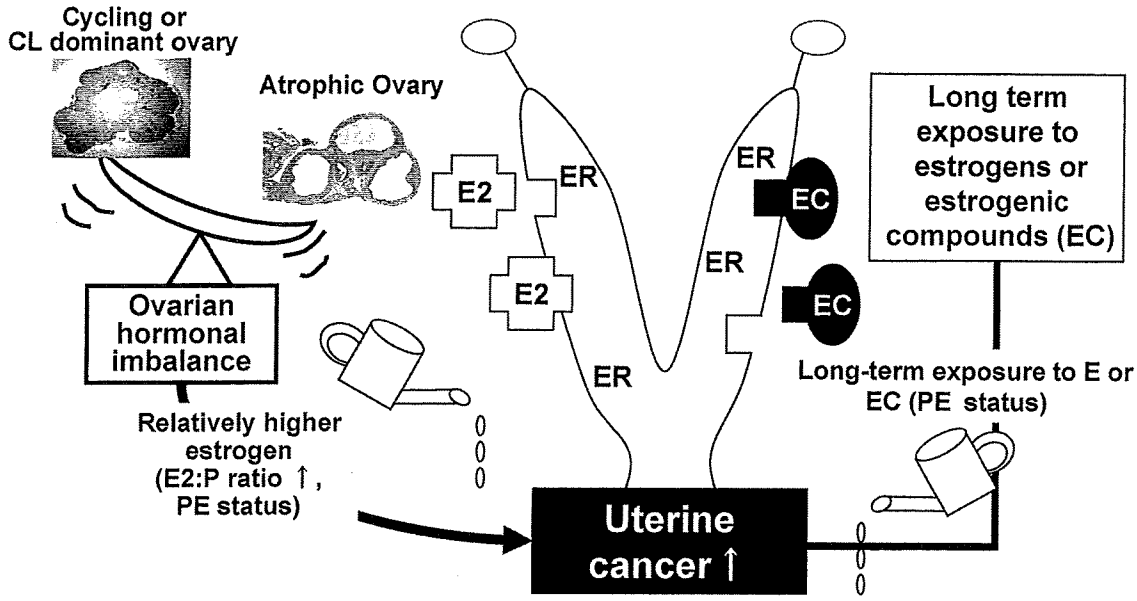


**Fig. 1.** Uterine carcinogenesis in the Donryu rat model with long-term exposure to a relatively high E2 status or estrogenic metabolites. CL, Corpora lutea; PE, persistent estrus determined by vaginal cytology; E2, 17$\beta$-estradiol; EC, estrogenic compounds; ER, estrogen receptors.

glucuronosyltransferase (UDP-GT), the rate-limiting enzyme in T4 metabolism in the rat[1,2], and thus leads to a decrease in blood T4[1,2]. Consequently, activation of the hypothalamo-pituitary-thyroid control system is activated with resultant elevation in the output of thyroid stimulating hormone (TSH). In 2-year or lifetime chronic toxicity/carcinogenicity studies, such long-term stimulation by PB and compensatory elevation of serum TSH levels finally results in thyroid follicular cell tumors[3,4]. Additionally, recent studies have proved that the decrease in serum thyroxine level by PB in rats is not necessarily dependent on increase in hepatic UDP-GT[5].

Induction of CYPs by non-genotoxic carcinogens is not thought to directly cause tumors, but many of the inducible forms are common to those responsible for metabolism of estrogen or other steroids, such as hydroxylation[6,7]. A number of chemicals such as environmental pollutants and dietary supplements[8–15] are inducers of such CYPs, especially of the CYP 1 or 3 family. Recently much attention has been paid to 4-hydroxyestradiol (4HE), a hydroxylation metabolite of 17$\beta$-Estradiol (E2) that have been reported to show stronger carcinogenic potential than E2, its parent compound, with reference to production of DNA damage in humans and animals[16–19]. This may be of particular importance for endometrial adenocarcinomas in the uterine corpus[20], which are generally increasing in women residing in developed countries and are now a leading cause of cancer death. While naturally occurring endometrial adenocarcinomas are generally very rare in rats[21], Maekawa *et al.* found a high-incidence of spontaneous lesions in aged Donryu rats with close similarities to human tumors[22,23], and have subsequently established a rat model of uterine carcinogenesis[24]. Elevated binding of E2 or other estrogenic compounds to estrogen receptor (ER)$\alpha$ is also a trigger for uterine carcinogenesis process of rodents[25–28] (Fig. 1), although precise mechanisms remain to be determined.

The hypothesis assessed in the present review is that chemicals exerting no estrogenic activity themselves but inducing CYPs might modify estrogen-dependent tumor development, and that a new pathway driven by modulation of estrogen metabolism via CYPs inducer might contribute to uterine carcinogenesis in rats. For this purpose I briefly introduce features of endometrial adenocarcinomas in Donryu rats, and present recent supportive data regarding induction of uterine cancers by CYP inducers. Whereas the liver is the main target of estrogen metabolism, in situ modulation of metabolite formation by CYPs in the mammary gland or uterus has also been recently reported[16]. Therefore a discussion of the possibility of in situ induction of CYPs in the uterus is included.

## Morphological and Endocrinological Features of Endometrial Adenocarcinomas in Donryu Rats

Endometrial adenocarcinomas morphologically develop through multiple stages in rats, as in the human case[20,22,23]. In middle-aged Donryu female rats (approximately 10 months of age, and equivalent to the menopausal phase in women) atypical hyperplasias characterized by endometrial epithelial cell hyperplasias with slight cellular atypia begin to develop in the endometrium as localized foci of proliferation, then increasing in number and size, demonstrating cellular atypia,

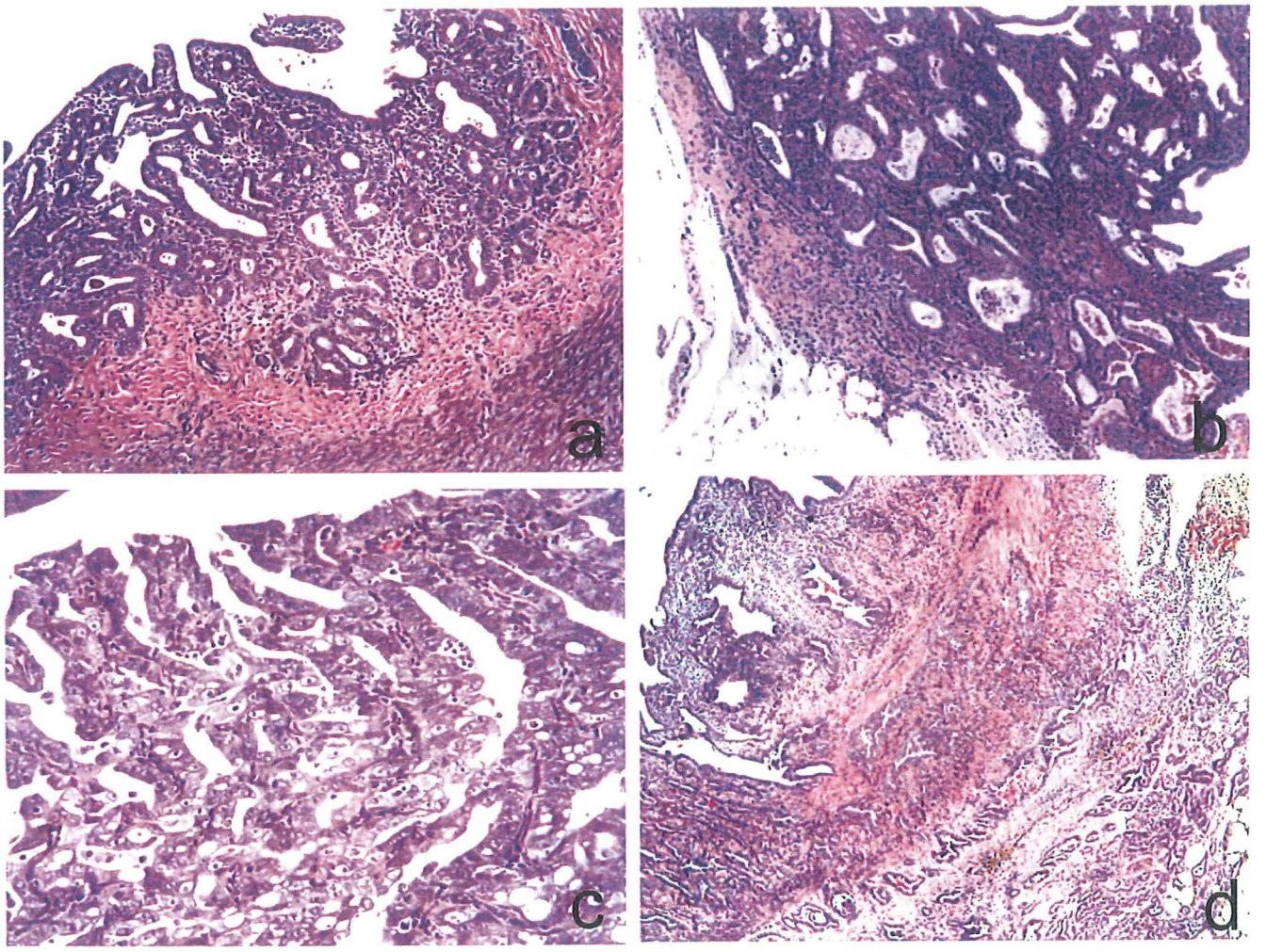


**Fig. 2.** Histopathological features of atypical endometrial hyperplasia (a), and well-differentiated (b, c) and moderately-differentiated (d) endometrial adenocarcinomas in Donryu rats occurred spontaneously (a, c) and induced by ENNG treatment (b, d). a, ×100; b; d, ×40; c, ×200. H-E.

with aging. In the next step, well-differentiated endometrial adenocarcinomas with morphological similarities to severe atypical hyperplasias but featuring invasion into the muscle layer or spread to the serosa in the uteri and/or the abdominal cavity, can be found. The incidence of such adenocarcinomas finally rises to 30–50% at 24 months of age. Furthermore, some adenocarcinomas demonstrate progression to moderately or poorly differentiated forms, increasing their malignancy. Based on the sequential development, the atypical hyperplasias are recognized as precursors of endometrial adenocarcinomas (Fig. 2).

A characteristic feature strongly linked to uterine carcinogenesis in this strain of rats is ovarian hormonal imbalance leading to elevation of serum E2 levels relative to progesterone (P), in line with uterine proliferating lesion development[27]. This imbalance leads to anovulation, morphologically detectable as atrophic ovaries with polycystic atretic follicles and loss of corpora lutea, eventually resulting in persistent estrus (PE) confirmable by vaginal cytology. PE first appears from 4 months of age in Donryu rats and affects most animals at 11 months, when other rat strains are still capable of reproduction. It should be noted that polycystic ovary is a high risk factor for uterine cancer in women[29–31].

## Establishment of a Uterine Endometrial Adenocarcinoma Model Using Donryu Rats

Based on the morphological and endocrinological similarities of uterine cancers in Donryu rats to those in women, a 2-stage uterine carcinogenesis model was established by Maekawa's group[32] to detect promoting or preventive effects of test-chemicals[24,27,33–35]. Briefly, in this model female Donryu rats at 10 or 11 weeks of age are initiated with *N-ethyl-N'-nitro-N-nitrosoguanidine* (ENNG) at the concentration of 20 mg/kg dissolved in polyethylene glycol and introduced into a unilateral uterine horn via vagina using a stainless steel catheter for initiation. Then the rats are exposed to test materials for 12 months and at 15 months of age are sacrificed to determine incidences or

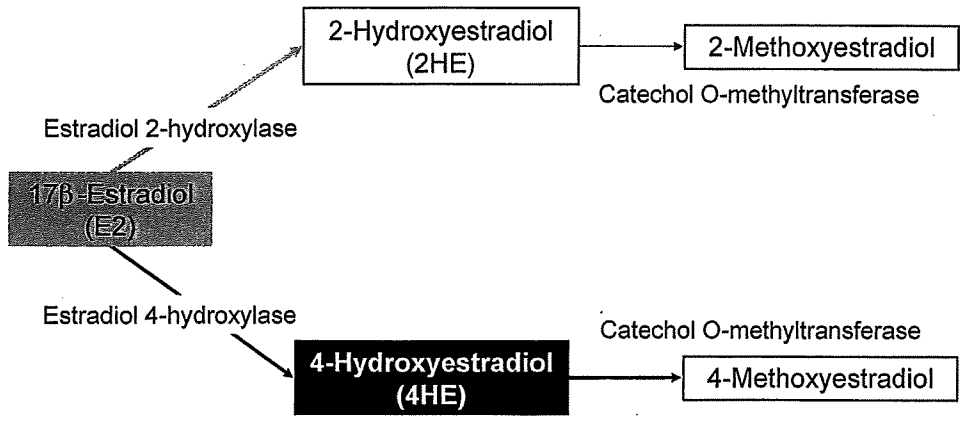


**Fig. 3.** Major pathway of catechol estrogen metabolism.

**Table 1.** Incidences (%) of Uterine Proliferative Lesions and Their Multiplicities at 15 Months of Age [Modified from ref. 52]

| | None | Atypical hyperplasia | | | Adenocarcinoma | Multiplicity(a) |
|---|---|---|---|---|---|---|
| | | Slight | Moderate | Severe | | |
| Control | 16.7 | 8.3 | 20.8 | 29.2 | 25.0 | 1.04 ± 0.62 |
| I3C 500 ppm | 3.3 | 6.8 | 10.0 | 23.2 | 56.7* | 1.50 ± 0.63* |
| Control | 11.1 | 11.1 | 38.9 | 16.7 | 22.2 | 1.17 ± 0.62 |
| I3C 2000 ppm | 5.6 | 11.1 | 27.8 | 11.1 | 44.4 | 1.78 ± 0.73** |
| E2 1 μg/kg | 0 | 18.8 | 12.4 | 18.8 | 50.0 | 1.50 ± 0.52 |
| 4HE 5 μg/kg | 0 | 0 | 31.2 | 6.3 | 62.5* | 1.69 ± 0.60** |

(a) Multiplicities are average numbers of uterine proliferative lesions per rat, mean ± SD.
*, **, Significantly different from the relevant control group ($p<0.05$ and 0.01, respectively. I3C, indole-3- carbinol.

multiplicities of uterine neoplastic lesions for comparison with controls (ENNG initiation only). The intrauterine treatment with a single dose of ENNG yields higher and earlier development of uterine neoplastic lesions than is the case with spontaneous development[32] and their morphologic features are extremely similarities between spontaneous and induced cases. In addition, the ENNG treatment is specific to the uteri, not affecting ovarian function and other organ tumorigenesis.

## Estrogen Metabolite or Catechol Estrogen Driven Uterine Carcinogenesis

In the rat liver, E2 is metabolized by estradiol 2- and 4-hydroxylases into the catechol estrogens, 2-hydroxyestradiol (2HE) and 4-hydroxyestradiol (4HE), respectively[7,36] (Fig. 3). 2-Hydroxylation of estradiol is the dominant pathway for catechol estrogen formation[7,36], and 2HE can bind to ERα, but with a markedly reduced affinity. This metabolite thus possesses much weaker hormonal potential than the parent hormone[37,38], and there is evidence that it is not a carcinogenic agent[39]. In contrast, 4HE, produced only in small amounts in the liver compared to 2HE, is hormonally active and can stimulate uterine growth with strong binding to estrogen receptors when injected into animals[7,36,40,41]. In

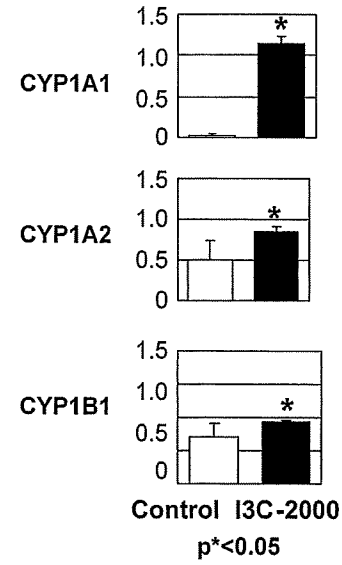


**Fig. 4.** Levels of expression of cytochrome P450s 1A1, 1A2 and 1B1 mRNA relative to GAPDH mRNA in the liver (calculated as %) in the rat at 15 months of age. Control, control group given basal diet only; I3C-2000, indole-3-carbinol at 2000 ppm in basal diet. [Modified from ref. 52]

addition, this catechol estrogen has been reported to be a stronger carcinogen than the parent E2 due to production of DNA damage[6,20], and causes tumor development in the kidney in hamsters[42], and possibly uterine and mammary gland neoplasia in human beings[18,19].

Recently, a number of dietary supplements extracted from vegetables have been produced, some of which are known to induce CYPs related to estrogen metabolism in the liver and estrogen dependent organs[18,40,43]. Since most of these products exert no direct estrogenic activity in target organs, they can only indirectly impact on estrogen dependent organ carcinogenesis through induction of CYPs and consequent modulation of estrogen metabolism. Indole-3-carbinol (I3C), an active ingredient of cruciferous vegetable, is reported to induce the CYP1 family enzymes in the liver[44,45], to thereby influence hydroxylation of estrogens and to suppress[39,46–49] or promote[50,51] carcinogenesis depending on the animal model. Regarding preventive effects, I3C acts as an anti-estrogen and can induce apoptosis, but precise mechanisms remain to be determined.

To determine estrogenic or anti-estrogenic activity of I3C in rat uteri, female Donryu rats were ovariectomized (OVX) at 9 weeks of age, and starting 2 weeks thereafter were assigned to nine groups receiving: only ovariectomy (controls); daily administration of 500 or 2000 ppm I3C in basal diet (I3C 500 or I3C 2000); 1 μg/kg E2 plus I3C 500 or I3C 2000; daily subcutaneous treatment with E2 at a dose of 1 μg/kg, and E2 metabolites such as 4HE at 5 μg/kg; 2HE at 5 μg/kg and 16α estradiol at 1 μg/kg[52]. After 2 weeks treatment, neither dose of I3C was found to have affected uterine weight or the height of the luminal epithelium in ovariectomized rats, with or without E2, and the estrogenic activity of 5 μg/kg 4HE was comparable to 1 μg/kg E2 treatment, while 2HE treatment had no activity. In addition, long-term treatment with dietary I3C at 500 or 2000 ppm did not disturb estrous cyclicity in Donryu rats, clearly demonstrating a lack of any estrogenic or anti-estrogenic activity, in line with results of uterotropic assays in OVX rats[52].

To clarify the effects of I3C on uterine adenocarcinoma development, 500 or 2000 ppm doses were administered to Donryu rats after ENNG initiation. The incidences and/or the multiplicities of lesions were significantly increased compared with those of the control group, as with 4-HE (Table 1)[52]. All uterine adenocarcinomas were of well-differentiated type, and morphological or biological malignancy was not influenced by the I3C treatment.

Histologically, hypertrophy of centrilobular hepatocytes was found in I3C treated groups, along with significantly increased CYP1A1, and to a lesser extent CYP1A2 and 1B1 mRNA expression compared to the control group (Figs. 4, 5). Immunohistochemically, CYP 1A1 and 1A2 were clearly demonstrable in the hepatocytes of centrilobular areas in the liver in both I3C-treated groups (Fig. 6), while mRNA and /or immunohistochemical findings for other cytochrome P450s such as 2B1, 3A1/2 or

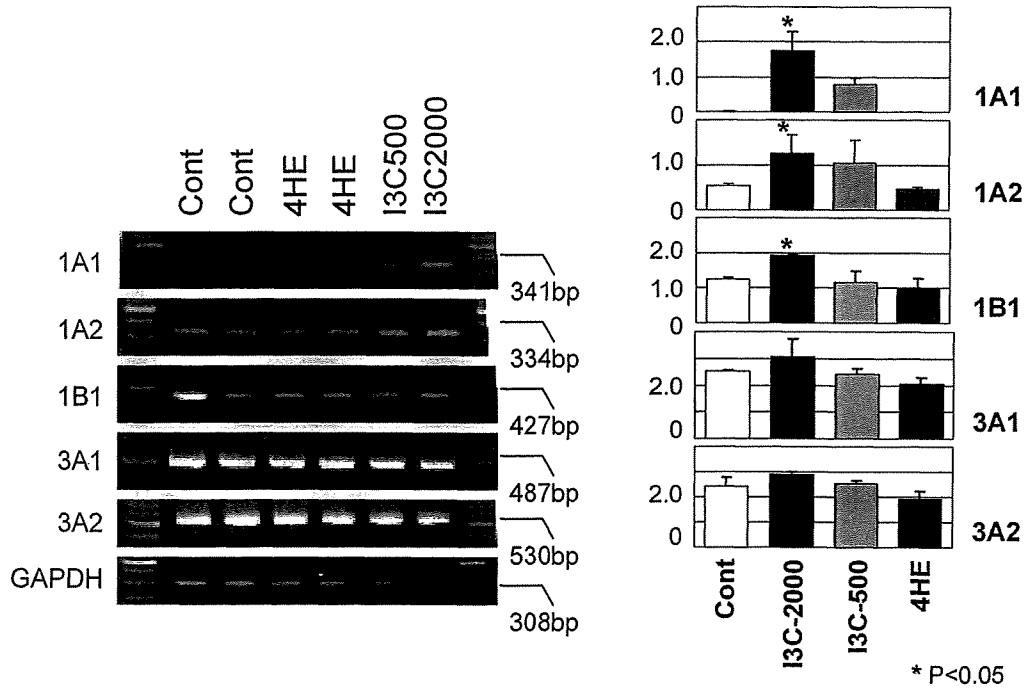


**Fig. 5.** mRNA Expression of cytochrome P450s 1A1, 1A2 1B1, 3A1and 3A2 and GAPDH (Left figure), and levels relative to GAPDH mRNA in the liver (calculated as % values) in ovariectomized rats (Right one). Control, control group given basal diet only; 4HE, daily subcutaneous injection of 5 μg/kg 4-hydroxyestradiol for 2 weeks; I3C-500 and I3C-2000, dietary indole-3-carbinol at 500 or 2000 ppm for 2 weeks, respectively; and I3C-2000+E2, concurrent treatment with I3C-2000 and daily subcutaneous injections of 1 μg/kg E2 for 2 weeks.

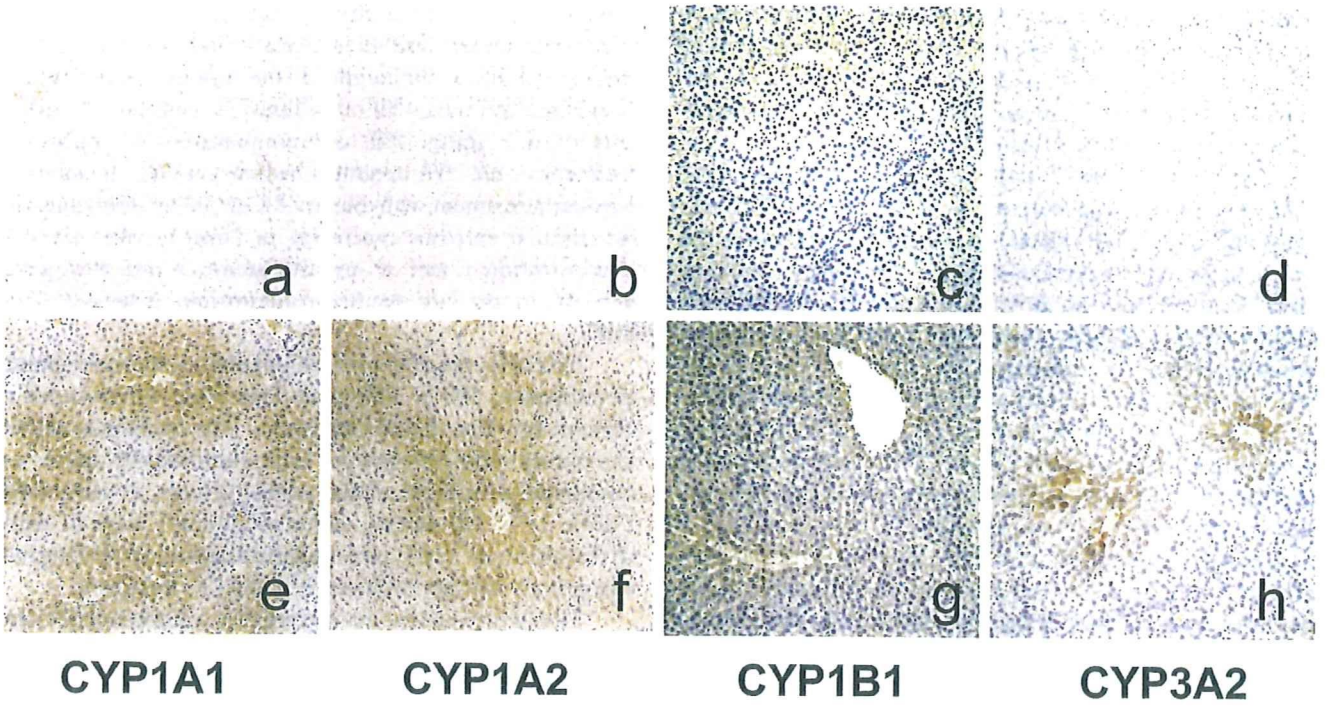


**Fig. 6.** Immunohistochemical localization of CYP1A1, 1A2, 1B1 and 3A2 in the livers of ovariectomized rats. a–d, Control group. e–h, dietary 2000 ppm I3C treated group. Note that centrilobular hepatocytes are strongly positive to CYP1A1 and 1A2, and slightly positive for 3A2, but negative for 1B1. Positive areas are visualized by diaminobenzidine, and counterstaining is with hematoxylin. ×100.

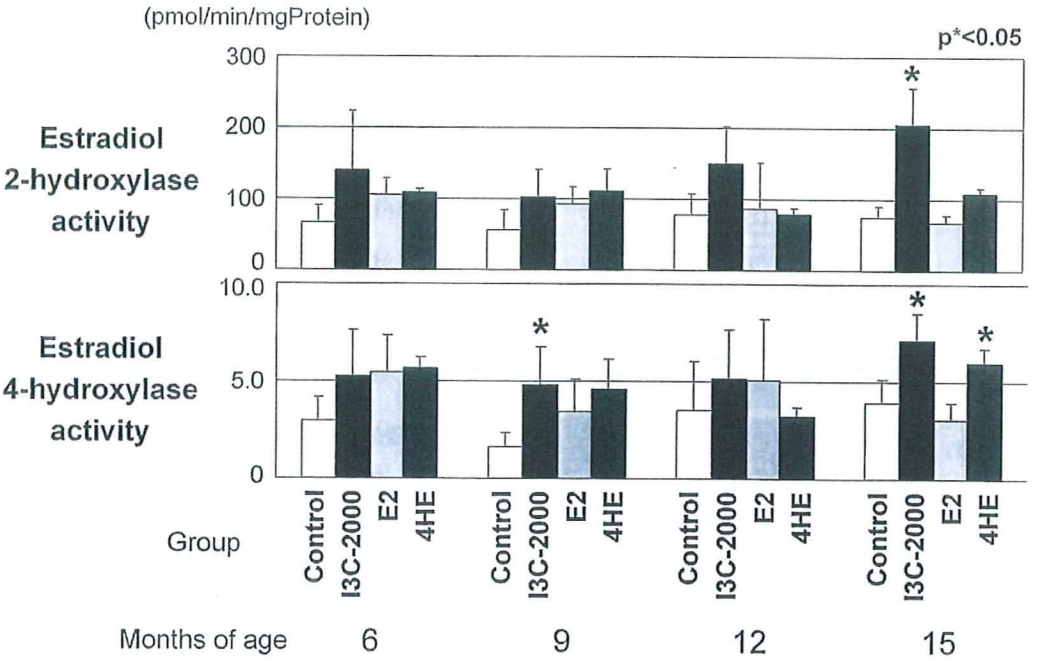


**Fig. 7.** Sequential changes in enzyme activity related to estrogen metabolism in the liver. Control, control group given basal diet only; I3C-2000, indole-3-carbinol at 2000 ppm in basal diet; E2, subcutaneous injection of 17$\beta$-estradiol at 1 $\mu$g/kg; 4HE, subcutaneous injection of 4-hydroxyestradiol at 5 $\mu$g/kg.

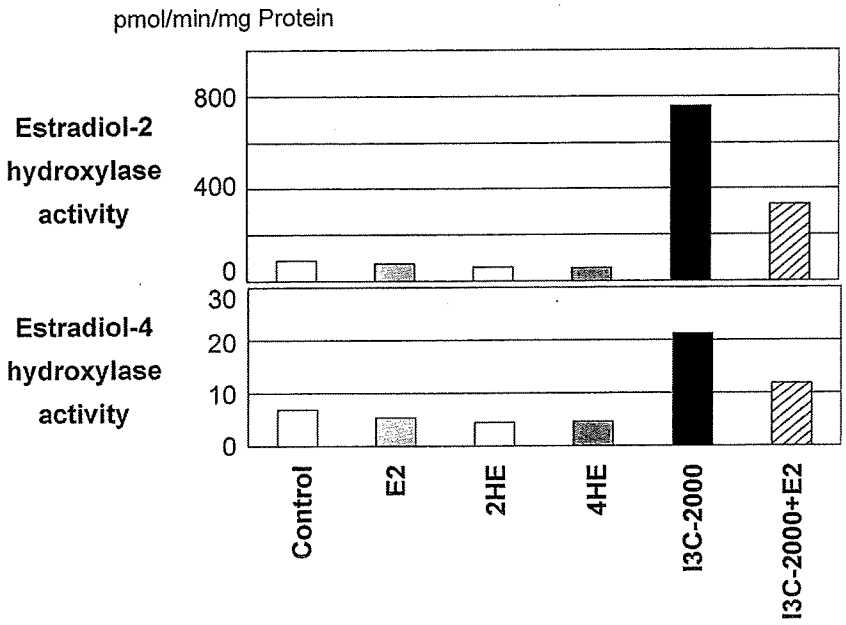


**Fig. 8.** Sequential changes in enzyme activity related to estrogen metabolism in the livers of ovariectomized rats. Control, control group given basal diet only; E2, subcutaneous injection of 1 μg/kg 17β-estradiol for 2 weeks; 2HE, subcutaneous injection of 5 μg/kg 2-hydroxyestradiol for 2 weeks; 4HE, subcutaneous injection of 5 μg/kg 4-hydroxyestradiol for 2 weeks; I3C-2000, indole-3-carbinol at 2000 ppm in basal diet for 2 weeks and I3C-2000+E2, concurrent treatment with I3C2000 ppm and E2.

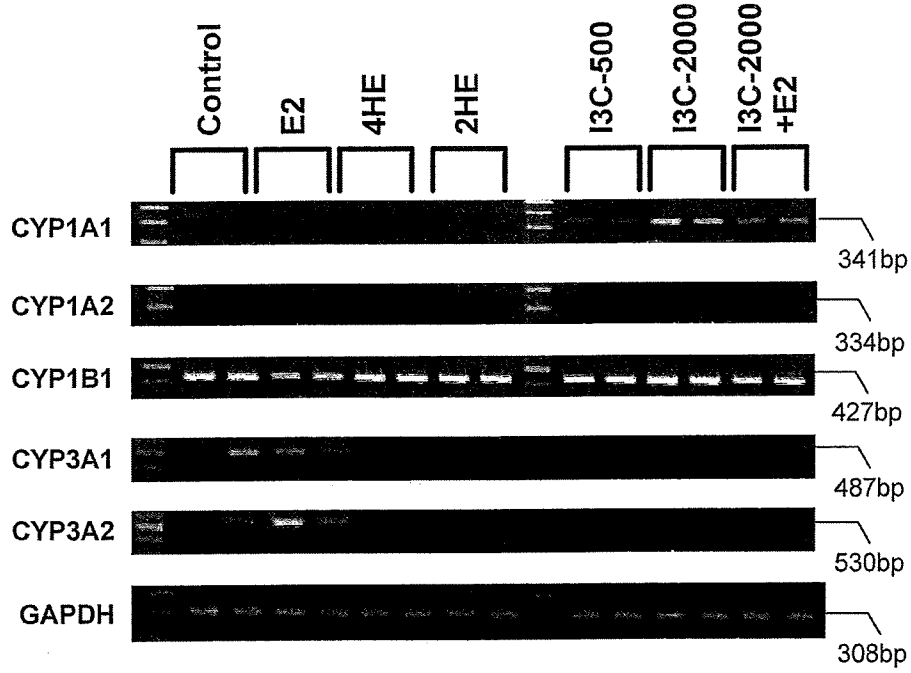


**Fig. 9.** mRNA Expression of cytochrome P450s 1A1, 1A2, 1B1, 3A1 and 3A2 and GAPDH in the uteri of ovariectomized rats. Control, control group given basal diet only; E2, Daily subcutaneous injection of 1 μg/kg 17β-estradiol for 2 weeks 4HE, daily subcutaneous injection of 5 μg/kg 4-hydroxyestradiol for 2 weeks; 2HE, daily subcutaneous injection of 5 μg/kg 2-hydroxyestradiol for 2 weeks; I3C-500 and I3C-2000, dietary indole-3-carbinol at 500 or 2000 ppm for 2 weeks, respectively; and I3C-2000+E2, concurrent treatment with I3C-2000 and E2.

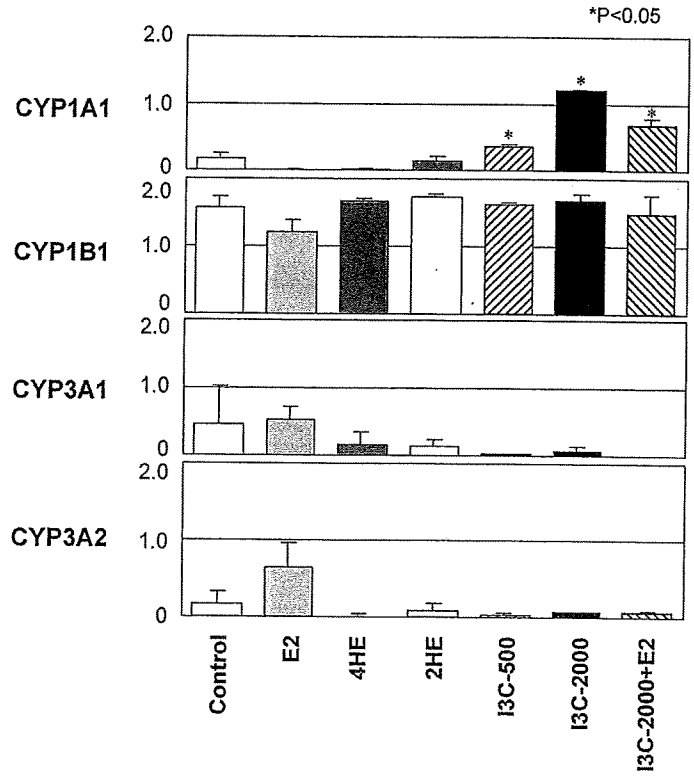


**Fig. 10.** mRNA Levels of the genes expressed in the Fig. 8 relative to GAPDH mRNA (calculated as %).

2C6 in the livers were comparable to the control case[52]. Measurement also demonstrated increase for estadiol 2- and 4- but not 16$\alpha$-hydroxylase activities related to estrogen metabolism (Figs. 7 and 8)[52]. In both of studies, 4-hydroxylation was particularly significantly increased.

## In Situ Expression of CYPs in the Uterus

Recently, extrahepatic CYP induction related to estrogen metabolism has been a focus of attention regarding the relationship to tumorigenesis in hamster kidney and human uterine tissue or myoma development[18,19,42]. In the hamster kidney, estrogen 2-hydroxylation is catalyzed by members of both CYP 1A and 3A families, the latter known to be related with steroid metabolism. CYP 1B1, which catalyzes E2 to 4-hydroxylation of estradiol, is a candidate key enzyme for development of human myomas. We have investigated CYP 1A1/2, 1B1, and 3A1/2-mRNA expression in the uterus of ovariectomozed Donryu rats treated with dietary I3C at 2000 ppm for 2 weeks[53], but no alteration in CYP 1A2, 1B1, 3A1 or 3A2 was observed (Figs. 9, 10). CYP 1A1 mRNA, but not its protein, was slightly up-regulated (Fig. 11). Additional studies of estradiol 4-hydroxylase activity or DNA adduct formation in the uterus need to be performed for confirmation, but the results do strongly suggest that I3C treatment does not affect in situ expression of CYPs in the rat uterus.

## Exploration of a New Pathway for Human Uterine Carcinogenesis

Induction of CYPs is not considered a direct trigger for promoting effects of non-genotoxic carcinogens. While we have no direct proof that the new pathway described in this review indeed contributes to human uterine carcinogenesis, CYP 1A1, 1A2 and 1B1 show high homology in their functions and control systems among mammals. In addition, a number of studies have indicated that CYP1B1 is a key enzyme for 4HE production through metabolism of E2 in both humans[54] and animals[8,15]. We have yet to determine which CYP enzyme is the most important for modulation of estrogen metabolism but further investigation of this area would appear to be clearly warranted.

In conclusion, our finding that I3C treatment promotes uterine endometrial adenocarcinoma development in the Donryu rat provides support for a new hypothesis of uterine carcinogenesis driven by modulation of estrogen metabolism in the liver due to CYP 1 family inducers which exert no estrogenic activity by themselves. The promoting effects are likely due to acceleration of 4-hydroxylation of E2, resulting in 4HE binding to ERs to afford a driving force for carcinogenic responses (Fig. 12).

**Acknowledgement:** This review basically summarizes a presentation in the symposium held at the 23rd Annual Meeting of the Japan Society of Toxicologic Pathology in

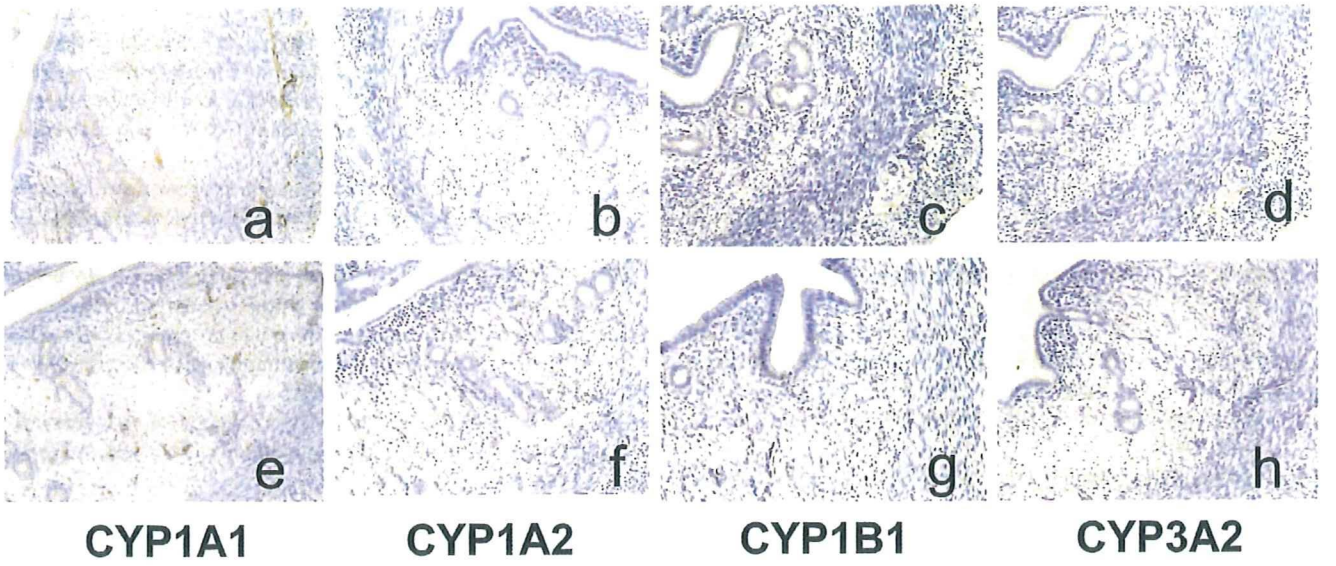


**Fig. 11.** Immunohistochemical localization of CYP1A1, 1A2, 1B1 and 3A2 in the uteri of ovariectomized rats. a–d, Control group. e–h, Dietary 2000 ppm I3C treated group for 2 weeks. Note lack of detectable positive reactions for these CYPs. Counterstaining was with hematoxylin. ×100.

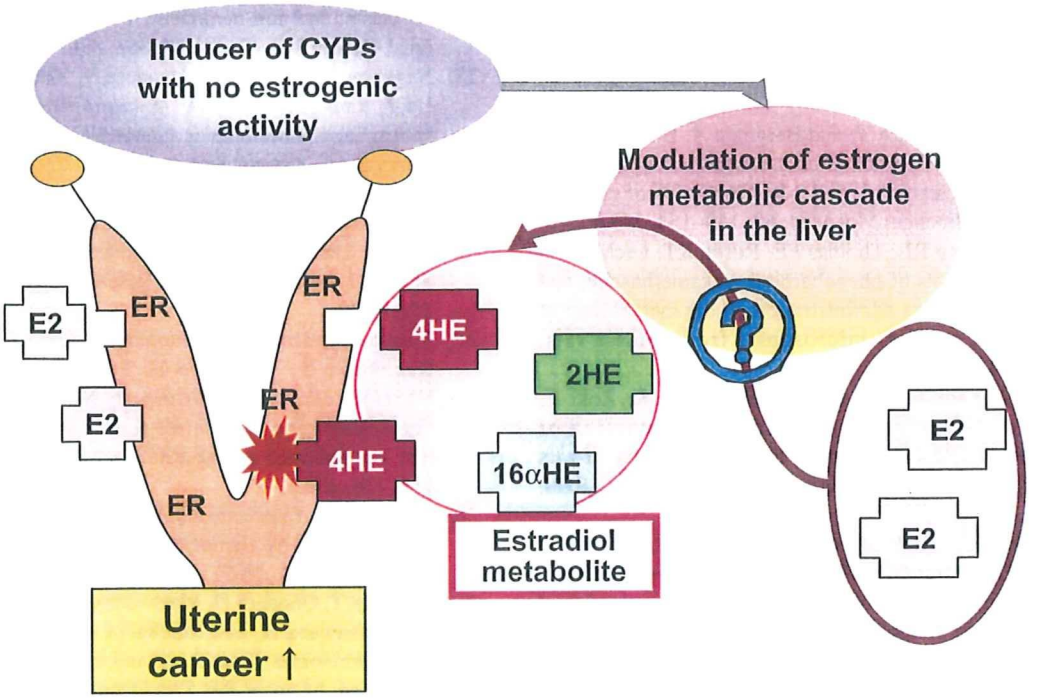


**Fig. 12.** A hypothesis: A pathway of uterine carcinogenesis driven by estrogen metabolite modulation through cytochrome P450s induction in the liver of rats.

Hamamatsu 2005. I sincerely thank the program committee, and particularly Dr. Kiyoshi Imai, the president of the Annual Meeting, for providing me with the opportunity to present the herein documented findings.

## References

1. McClain RM. The significance of hepatic microsomal enzyme induction and altered thyroid function in rats: implications for thyroid gland neoplasia. Toxicol Pathol. **17**: 294–306. 1989.

2. Capen CC. Mechanistic data and risk assessment of selected toxic end points of the thyroid gland. Toxicol Pathol. **25**: 39–48. 1997.
3. Barter RA and Klaassen CD. Reduction of thyroid hormone levels and alteration of thyroid function by four representative UDP-gluduronosyltransferase inducers in rats. Toxcol Appl Pharmacol. **128**: 9–17. 1994.
4. Liu J, Liu Y, Barter RA, and Klaassen CD. Alteration of thyroid homeostasis by UDP-glucuronosyltransferase inducers in rats: a dose-response study. J Pharmacol Exp Ther. **273**: 977–985. 1995.
5. Kato Y, Suzuki H, Ikushiro S, Yamada S, and Degawa M. Decrease in serum thyroxine level by phenobarbital in rats is not necessary dependent on increase in hepatic UDP-glucuronosyltranserse. Drug Metab Desposition. **33**: 1608–1612. 2005.
6. Dannan GA, Porubek DJ, Nelson SD, Waxman DJ, and Guengerich EP. 17$\beta$-estradiol 2- and 4-hydroxylation catalyzed by rat hepatic cytochrome P-450: roles of individual forms, inductive effects, developmental patterns, and alterations by gonadectomy and hormone replacement. Endocrinol. **118**: 1952–1960. 1986.
7. Zhu BT and Conney AH. Functional role of estrogen metabolism in target cells: review and perspectives. Carcinogenesis. **19**: 1–27. 1998.
8. Badawi AF, Cavalieri EL, and Rogan EG. Effect of chlorinated hydrocarbons on expression of cytochrome P450 1A1, 1A2 and 1B1 and 2- and 4-hydroxylation of 17$\beta$-estradiol in female Sprague-Dawley rats. Carcinogenesis. **21**: 1593–1599. 2000.
9. Segura-Aguilar J, Castro V, and Bergman A. Effects of four organohalogen environmental contaminants on cytochrome P450 forms that catalyze 4- and 2-hydroxylation of estradiol in the rat liver. Biochem Mol Med. **60**: 149–154. 1997.
10. Suchar LA, Chang RL, Thomas PE, Rosen RT, Lech J, and Conney AH. Effects of phenobarbital, dexamethasone, and 3-methylcholanthrene administration on the metabolism of 17$\beta$-estradiol by liver microsomes from female rats. Endocrinol. **137**: 663–676. 1996.
11. Hatanaka N, Yamazaki H, Kizu R, Hayakawa K, Aoki Y, Iwanari M, Nakajima M, and Yokoi T. Induction of cytochrome P450 1B1 in lung, liver and kidney of rats exposed to diesel exhaust. Carcinogenesis. **22**: 2033–2038. 2001.
12. Santostefano MJ, Richardson VM, Walker NJ, Blanton J, Lindros KO, Lucier GW, Alcasey SK, and Birnbaum LS. Dose-dependent localization of TCDD in isolated centrilobular and periportal hepatocytes. Toxicol Sci. **52**: 9–19. 1999.
13. Walker NJ, Portier CJ, Lax SF, Crofts FG, Li Y, Lucier GW, and Sutter TR. Characterization of the dose-response of CYP1B1, CYP1A1, and CYP1A2 in the liver of female Sprague-Dawley rats following chronic exposure to 2,3,7,8-tetrachlorodibenzo-p-dioxin. Toxiol Appl Pharmacol. **154**: 279–286. 1999.
14. Counmoul X, Diry M, Robillot C, and Barouki R. Differential regulation of cytochrome P450 1A1 and 1B1 by a combination of dioxin and pesticides in the breast tumor cell line MCF-7. Cancer Res. **61**: 3942–3948. 2001.
15. Shimada T, Hayes CH, Yamazaki H, Amin S, Hecht SS, Guengerich FP and Sutter TR. Activation of chemically diverse procarcinogens by human cytochrome P-450 1B1. Cancer Res. **56**: 2979–2984. 1996.
16. Horn TL, Reichet MA, Bliss RL, and Malejka-Giganti D. Modulations of P450 mRNA in liver and mammary gland and P450 activities and metabolism of estrogen in liver by treatment of rats with indole-3-carbinol. Biochem Pharmacol. **64**: 393–404. 2002.
17. Yager JD and Liehr JG. Molecular mechanisms of estrogen carcinogenesis. Annu Rev Pharmacol Toxicol. **36**: 203–232. 1996.
18. Liehr JG, Ricci MJ, Jefcoate CR, Hannigan EV, Hokanson JA, and Zhu BT. 4-Hydroxylation of estradiol by human uterine myometrium and myoma microsomes: implications for the mechanism of uterine tumorigenesis. Proc Natl Acad Sci USA. **92**: 9220–9224. 1995.
19. Liehr JG and Ricci MJ. 4-Hydroxylation of estrogens and markers of human mammary tumors. Proc Natl Acad Sci USA. **93**: 3294–3296. 1996.
20. Sherman ME. Theories of endometrial carcinogenesis: a multidisciplinary approach. Modern Pathol. **13**: 295–308. 2000.
21. Haseman JK, Halley JR, and Morris RW. Spontaneous neoplasm incidence in Fischer 344 rats and B6C3F1 mice in two-year carcinogenicity studies: National Toxicology Program Update. Toxicol Pathol. **26**: 428–441. 1998.
22. Maekawa A, Onodera H, Tanigawa H, Furuta K, Kanno J, Matsuoka C, Ogiu T, and Hahashi Y. Spontaneous neoplastic and non-neoplastic lesions in aging Donryu rats. Jpn J Cancer Res (Gann). **77**: 882–890. 1986.
23. Nagaoka T, Takeuchi M, Onodera H, Matsushima Y, Ando-Lu J, and Maekawa A. A sequential observation of spontaneous endometrial adenocarcinoma development in Donryu rats. Toxicol Pathol. **22**: 261–269. 1994.
24. Yoshida M and Maekawa A. Uterine carcinogenesis based on estrogen or metabolite driven pathways in the Donryu rats. In: Carcinogenesis and Modification of Carcinogenesis, Tanaka T and Tsuda H (eds). Research Signpost, India. 135–151. 2005.
25. Katsuda S, Yoshida M, Kuroda H, Ando J, Takahashi M, Kurokawa Y, Watanabe G, Taya K, and Maekawa A. Uterine adenocarcinoma in N-ethyl-N'-nitro-N-nitrosoguanidine-treated rats with high-dose exposure to p-tert -octylphenol during adulthood. Jpn J Cancer Res. **93**: 117–124. 2002.
26. Maekawa A, Takahashi M, Ando J, and Yoshida M. Uterine carcinogenesis by chemicals/hormones in rodents. J Toxicol Pathol. **12**: 1–11. 1999.
27. Nagaoka T, Onodera H, Matsushima Y, Todate A, Shibutani M, Ogasawara H, and Maekawa A. Spontaneous uterine adenocarcinomas in aged rats and their relation to endocrine imbalance. J Cancer Res Clin Oncol. **116**: 623–628. 1990.
28. Nagaoka T, Takeuchi M, Onodera H, Mitsumori K, Lu J, and Maekawa A. Experimental induction of uterine adenocarcinoma in rats by estrogen and N-methyl-N-nitrosourea. In Vivo. **7**: 525–530. 1993.
29. Balen A. Polycystic ovary syndrome and cancer. Hum Reprod Update. **7**: 522–525. 2001.
30. Hardiman P, Pillary OC, and Atiomo W. Polycystic ovary syndrome and endometrial carcinoma. Lancet. **361**: 1810–1812. 2003.
31. Soliman PT, Oh JC, Schrmeler KM, Sun CC, Slomovitz BM, Gershenson DM, Burke TW, and Lu KH. Risk factors for young premanopausal women with endometrial cancer.

Obstet Gynecol. **105**: 575–580. 2005.
32. Ando-Lu J, Takahashi M, Imai S, Ishihara R, Kitamura T, Iijima T, Takano S, Nishiyama K, Suzuki K, and Maekawa A. High-yield induction of endometrial adenocarcinomas in Donryu rats by a single intra-uterine administration of N-ethyl-N'-nitro-N-nitrosoguanidine. Jpn J Cancer Res. **85**: 789–793. 1994.
33. Katsuda S, Yoshida M, Saarinen N, Smeds A, Nakae D, Santti R, and Maekawa A. Chemopreventive effects of hydroxymatairesinol on uterine carcinogenesis in Donryu rats. Exp Biol Med. **229**: 417–424. 2004.
34. Nishiyama K, Ando-Lu J, Nishimura S, Takahashi M, Yoshida M, Sasahara K, Miyajima K, and Maekawa A. Initiating and promoting effects of concurrent oral administration of ethylenethiourea and sodium nitrite on uterine endometrial adenocarcinoma development in Donryu rats. In Vivo. **2**: 363–368. 1998.
35. Yoshida M, Kudoh K, Katsuda S, Takahashi M, Ando J, and Maekawa A. Inhibitory effects of uterine endometrial carcinogenesis in Donryu rats by tamoxifen. Cancer Lett. **134**: 43–51. 1998.
36. Liehr JG. Is estradiol a genotoxic mutagenic carcinogen? Endoc Rev. **21**: 40–54. 2000.
37. Van Aswegen CH, Purdy RH, and Wittliff JL. Binding to 2-hydroxyestradiol and 4-hydroxyestradiol to estrogen receptor human breast cancers. J Steroid Biochem. **32**: 485–492. 1989.
38. MacLusky NJ, Barnea ER, Clark CR, and Naftolin F. Catechol estrogens and estrogen receptors. In: Catechol Estrogens, Merrian GR, and Lipsett MB (eds). Raven Press, New York, 151–165. 1983.
39. Kojima T, Takana T, and Mori H. Chemoprevention of spontaneous endometrial cancer in female Donryu rats by dietary indole-3-carbinol. Cancer Res. **54**: 1446–1449. 1994.
40. Marticci CP and Fishman J. P450 enzymes of estrogen metabolism. Pharmacol Ther. **57**: 237–257. 1993.
41. Liehr JG, Fang WF, Sirbasku DA, and Ulubelen AA. Carcinogenicity of catechol estrogens in Syrian hamster. J Steroid Biochem. **24**: 353–356. 1986.
42. Hammond DK, Zhu BT, Wang MY, Ricci MJ, and Liehr JG. Cytochrome P450 metabolism of estradiol in hamster liver and kidney. Toxicol Appl Pharmacol. **145**: 54–60. 1997.
43. Jang EH, Park YC, and Chung WG. Effects of dietary supplements on induction and inhibition of cytochrome P450s protein expression in rats. Food Chem Toxicol. **42**: 1749–1756. 2004.
44. Jongen W. Glucosinolates in brassica: occurrence and significance as cancer-modulating agents. Proc Nutr Soc. **55**: 433–446. 1996.
45. Bonnesen C, Eggleston IM, and Hayes JD. Dietary indoles and isothiocyanates that are generated from cruciferous vegetables can both stimulate apoptosis and confer protection against DNA damage in human colon cell lines. Cancer Res. **61**: 6120–6130. 2001.
46. Bradlow HL, Michnovicz JJ, Telang NT, and Osborne MP. Effects of dietary indole-3-carbinol on estradiol metabolism and spontaneous mammary tumors in mice. Carcinogenesis. **12**: 1571–1574. 1991.
47. Meng Q, Yuan F, Goldberg ID, Rosen EM, Auborn K, and Fan S. Indole-3-carbinol is a negative regulator of estrogen receptor-$\alpha$ signaling in human tumor cells. J Nutr. **130**: 2927–2931. 2000.
48. Michnovicz JJ and Bradlow HL. Induction of estradiol metabolism by dietary indole-3-carbinol in humans. J Natl Cancer Inst. **82**: 947–949. 1990.
49. Michnovicz JJ, Adlecreutz H, and Bradlow HL. Changes in levels of urinary estrogen metabolites after oral indole-3-carbinol treatment in humans. J Natl Cancer Inst. **89**: 718–823. 1997.
50. Kang JS, Kim DJ, Ahn B, Nam KT, Kim KS, Choi M, and Jang DD. Post-initiation treatment of Indole-3-carbinol did not supress N-methyl-N-nitrosourea induced mammary carcinogenesis in rats. Can Lett. **169**: 147–154. 2001.
51. Stoner G, Casto B, Ralston S, Roebuck B, Pereira C, and Bailey G. Development of a multi-organ rat model for evaluating chemopreventive agents: efficacy of indole-3-carbinol. Carcinogenesis. **23**: 265–272. 2002.
52. Yoshida M, Katashima S, Ando J, Tanaka T, Uematsu F, Nakae D, and Maekawa A. Dietary indole-3-carbinol promotes endometrial adenocarcinoma development in rats initiated with N-ethyl-N'-nitrosoguanidine, with induction of cytochrome P450s in the liver and consequent modulation of estrogen metabolism. Carcinogenesis. **11**: 2257–2264. 2004.
53. Yoshida M, Nakae D, and Maekawa A. Expression profiles of cytochrome P450 enzymes in the uterus and liver of female rats treated with indole-3-carbinol. J Toxicol Sci. **30 (Supplement)**: S83. 2005.
54. Tsuchiya Y, Nakajima M, Kyo S, Kanaya T, Inoue M, and Yokoi T. Human CYP1B1 is regulated by estradiol via estrogen receptor. Cancer Res. **64**: 3119–3125. 2004.

MOLECULAR AND CELLULAR BIOLOGY, May 2006, p. 3610–3624 Vol. 26, No. 9
0270-7306/06/$08.00+0 doi:10.1128/MCB.26.9.3610–3624.2006


# Disruption of Spermatogenic Cell Adhesion and Male Infertility in Mice Lacking TSLC1/IGSF4, an Immunoglobulin Superfamily Cell Adhesion Molecule†

Daisuke Yamada,[1] Midori Yoshida,[2] Yuko N. Williams,[1] Takeshi Fukami,[1] Shinji Kikuchi,[1] Mari Masuda,[1] Tomoko Maruyama,[1] Tsutomu Ohta,[3] Dai Nakae,[2] Akihiko Maekawa,[2] Tadaichi Kitamura,[4] and Yoshinori Murakami[1]*

*Tumor Suppression and Functional Genomics Project[1] and Genetics Division,[3] National Cancer Center Research Institute, Tokyo, Japan; Department of Pathology, Sasaki Institute, Sasaki Foundation, Tokyo, Japan[2]; and Department of Urology, Graduate School of Medicine, University of Tokyo, Tokyo, Japan[4]*

Received 5 August 2005/Returned for modification 1 October 2005/Accepted 30 January 2006

**TSLC1/IGSF4, an immunoglobulin superfamily molecule, is predominantly expressed in the brain, lungs, and testes and plays important roles in epithelial cell adhesion, cancer invasion, and synapse formation. We generated *Tslc1/Igsf4*-deficient mice by disrupting exon 1 of the gene and found that *Tslc1*$^{-/-}$ mice were born with the expected Mendelian ratio but that *Tslc1*$^{-/-}$ male mice were infertile. In 11-week-old adult *Tslc1*$^{-/-}$ mice, the weight of a testis was 88% that in *Tslc1*$^{+/+}$ mice, and the number of sperm in the semen was approximately 0.01% that in *Tslc1*$^{+/+}$ mice. Histological analysis revealed that the round spermatids and the pachytene spermatocytes failed to attach to the Sertoli cells in the seminiferous tubules and sloughed off into the lumen with apoptosis in the *Tslc1*$^{-/-}$ mice. On the other hand, the spermatogonia and the interstitial cells, including Leydig cells, were essentially unaffected. In the *Tslc1*$^{+/+}$ mice, TSLC1/IGSF4 expression was observed in the spermatogenic cells from the intermediate spermatogonia to the early pachytene spermatocytes and from spermatids at step 7 or later. These findings suggest that TSLC1/IGSF4 expression is indispensable for the adhesion of spermatocytes and spermatids to Sertoli cells and for their normal differentiation into mature spermatozoa.**

Infertility is estimated to affect about 5% of adult human males. However, approximately 75% of these cases are diagnosed as idiopathic because the molecular mechanisms underlying these defects have not been elucidated (17, 20). Recently, male infertility has been reported as a phenotype in mice that are deficient in various single genes, providing knowledge about possible molecular targets causing male infertility in humans. So far, more than 80 genes have been identified as essential for male fertility in humans and mice (11). These genes encode a variety of proteins, including signal transduction molecules, transcription factors, metabolic enzymes, transmembrane proteins, and cytoskeletal proteins. From the pathological point of view, the causes of male infertility can be grouped into the following three categories, depending on the stage of cell differentiation affected: defects in the primordial germ cells, those in the spermatogenic cells, and those in the spermatozoa. Among these defects, abnormalities in the genes involved in the primordial germ cells and the resultant developmental defects in the reproductive organs are relatively rare, probably because such defects often cause embryonic lethality. On the other hand, spermatogenesis, a series of spermatogenic cell differentiation steps from spermatogonia to mature spermatozoa in the testes, is considered the major target of defects in male infertility. In fact, about 70% of the genes essential for male fertility are involved in this process. Another 20% of the genes have been shown to play a role in the formation, motility, or fertilizing ability of spermatozoa.

Spermatogenesis can be further divided into the following three phases: (i) the proliferative phase, in which the spermatogonia undergo rapid successive divisions; (ii) the meiotic phase, in which the spermatocytes produce cells with haploid chromosome content; and (iii) the spermiogenic phase, in which the spermatids differentiate into mature spermatozoa, which can fertilize the egg (15).

We have previously identified the *TSLC1/IGSF4* gene on chromosome 11q23.2 as a tumor suppressor in sporadic lung cancer by its activity in the suppression of tumorigenicity in nude mice by a lung cancer cell line, A549 (7). *TSLC1/IGSF4* is predominantly expressed in the brain, lungs, and testes and is followed by most epithelial and neuronal tissues, while the loss of its expression through promoter methylation associated with a loss of heterozygosity is observed in a variety of human tumors, including lung, esophageal, pancreatic, breast, and prostate cancers, especially in tumors with aggressive behavior (12). The TSLC1/IGSF4 protein belongs to immunoglobulin superfamily cell adhesion molecules (IgCAMs) containing three Ig-like loops in the extracellular domain and mediates cell-to-cell adhesion through homophilic and heterophilic interactions in a $Ca^{2+}$- and $Mg^{2+}$-independent manner (10). A mouse orthologue of the *Tslc1/Igsf4* gene shows extremely high homology to human *TSLC1/IGSF4*, with 97% identity in the

* Corresponding author. Mailing address: Tumor Suppression and Functional Genomics Project, National Cancer Center Research Institute, 5-1-1 Tsukiji, Chuo-ku, Tokyo 104-0045, Japan. Phone: 81-3-3547-5295. Fax: 81-3-5565-9535. E-mail: ymurakam@gan2.res.ncc.go.jp.

† Supplemental material for this article may be found at http://mcb.asm.org/.

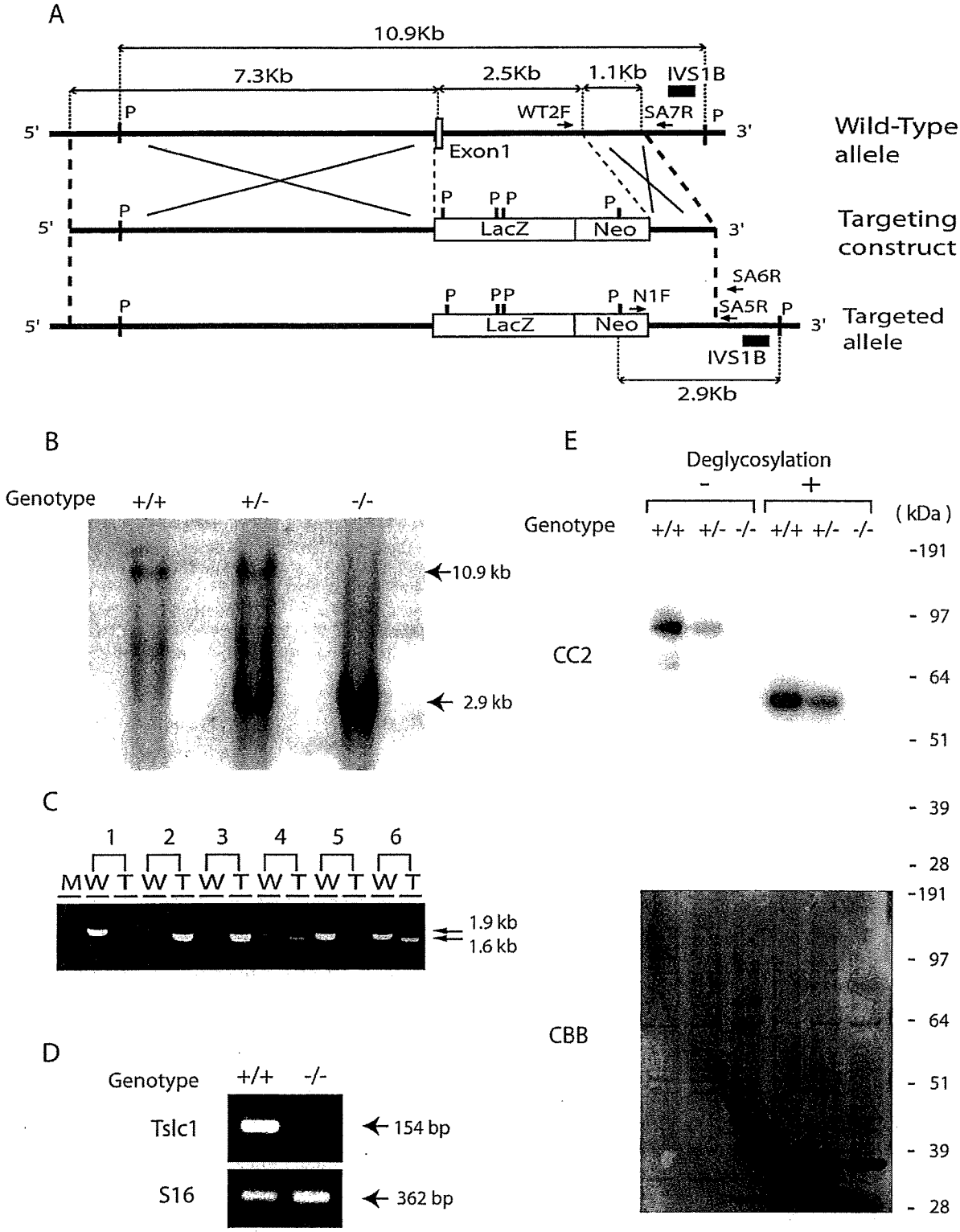


FIG. 1. Generation of *Tslc1*$^{-/-}$ mice. (A) Wild-type allele, targeting construct, and targeted allele of the *Tslc1/Igsf4* gene. An open box and solid lines indicate an exon and introns, respectively. IVS1B is a genomic fragment used as a probe for Southern blotting. WT2F and SA7R are the primers for PCR complementary to the wild-type genomic sequence of the *Tslc1/Igsf4* gene, while N1F and SA5R are the PCR primers complementary to the targeted allele. P, restriction site of PvuII. (B) Southern blot analysis of the wild-type and targeted alleles of *Tslc1/Igsf4*. Genomic DNA was digested with a restriction enzyme, PvuII, blotted, and hybridized with a probe, IVS1B. Fragments of 10.9 kb and 2.9 kb were derived from the wild-type and targeted alleles, respectively. (C) PCR analysis for monitoring inheritance of the targeted allele of *Tslc1/Igsf4* in the progeny of the *Tslc1*$^{+/-}$ intercross. W and T indicate the wild-type allele (1.9 kb) and the targeted allele (1.6 kb), respectively. M, molecular marker. (D) RT-PCR analysis of *Tslc1/Igsf4* in the testes from *Tslc1*$^{+/+}$ and *Tslc1*$^{-/-}$ mice. A fragment of 154 bp corresponds to exons 1 to 3 of the *Tslc1/Igsf4* mRNA. A ribosomal protein gene, S16, served as a control endogenous gene. (E) Western blotting of testis lysates, with or without treatment for deglycosylation, from *Tslc1*$^{+/+}$, *Tslc1*$^{+/-}$, and *Tslc1*$^{-/-}$ mice. The filter was hybridized with the anti-TSLC1/IGSF4 antibody CC2 (top) or stained with Coomassie brilliant blue (CBB; bottom).

overall amino acid sequences, suggesting that TSLC1/IGSF4 plays an important role during evolution (3).

Wakayama et al. independently cloned *SgIGSF*, a mouse orthologue of *TSLC1/IGSF4*, by scanning the database of mouse expressed sequence tags and selecting a sequence homologous to the neural cell adhesion molecules (19). Expression of this molecule, SgISGF/IGSF4, was detected in the membranes of spermatogenic cells in two distinct phases, one from the intermediate spermatogonia through the early pachytene spermatocytes and the other from step 7 spermatids to step 16 residual bodies. These findings suggest that, in the testes, SgIGSF/IGSF4 may be involved in spermatogenesis (18).

To elucidate the physiological function of TSLC1/IGSF4, we generated mutant mice lacking the *Tslc1/Igsf4* gene. We report in the present study that *Tslc1/Igsf4*-deficient mice are born without any overt abnormalities but that the males are infertile.

## MATERIALS AND METHODS

**Generation of mice lacking the *Tslc1/Igsf4* gene.** An 11-kb mouse genomic DNA fragment containing exon 1 of the *Tslc1/Igsf4* gene was cloned from the mouse 129Sv/Ev bacterial artificial chromosome genomic library by hybridization with a radiolabeled probe generated from the mouse genomic sequence around exon 1 of the *Tslc1/Igsf4* gene (3). From this clone, a fragment of 7.3 kb upstream of exon 1 and one of 1.1 kb within intron 1 were subcloned, and the targeting construct was generated by inserting these fragments into the 5′ and 3′ sites of the LacZ-neomycin (Neo) resistance gene cassette, respectively (Fig. 1A). The genomic fragment of 2.5 kb containing exon 1 of the *Tslc1/Igsf4* gene, which was replaced by the LacZ-Neo cassette, starts with the sequence 5′-CCGACATGG CGAGTGCTGTGCTGCCGAGCGGATCCCAGTGTGCGGCGG-3′ and ends with 5′-TAGGGCTTTGCTAAGACTCTCTCTCAAACTGTATAC-3′. By homologous recombination, therefore, it was expected that all coding sequences of exon 1 and the 5′ region of intron 1 of the *Tslc1/Igsf4* gene were deleted, whereas the LacZ gene as well as the neomycin resistance gene was inserted into the targeted allele so that the expression of the LacZ gene could be regulated by the endogenous promoter of the *Tslc1/Igsf4* gene (Fig. 1A). Ten micrograms of the targeting vector was linearized by NotI, transfected into 129Sv/Ev iTL1 embryonic stem (ES) cells by electroporation, and selected with G418. Among the 300 neomycin-resistant cells obtained, two ES cells that had undergone homologous recombination were identified by PCR analysis using primers N1F and SA6R (Fig. 1A). The sequences of the primers are listed in Table S1 in the supplemental material. These targeted ES cells were microinjected into C57BL/6J blastocysts to generate seven male chimeras and nine female chimeras. The chimeric mice were then mated with C57BL/6J mice to obtain offspring that were heterozygous for the targeted inactivation of the *Tslc1/Igsf4* gene. Germ line transmission of the targeted allele was confirmed by Southern blotting and monitored by PCR, in which the wild-type fragment was generated by primers WT2F and SA7R, while the targeted fragment was generated by primers N1F and SA5R (Fig. 1A). All animals used in this study were handled in compliance with the National Cancer Center Research Institute's guidelines for the use of animals.

**Southern blotting.** Mouse genomic DNA was extracted by the phenol-chloroform extraction method. Five micrograms of genomic DNA was digested with PvuII, subjected to electrophoresis through a 0.8% agarose gel, and blotted onto a Hybond-N$^+$ membrane (Amersham Biosciences, Buckinghamshire, United Kingdom) using the alkaline transfer method. A fragment, IVS1A, corresponding to the 1,021-bp genomic DNA in intron 1 of the murine *Tslc1/Igsf4* gene, was generated by PCR using primers 16205F and 17225R (see Table S1 in the supplemental material) and cloned into a TOPO cloning vector (Invitrogen, Carlsbad, CA) to obtain pmIVS1A. Fragment IVS1B, of 436 bp, was generated by digesting pmIVS1A DNA with BstXI and was used as a probe for Southern blotting. Radiolabeling of the probe was carried out with [$^{32}$P]dCTP using the Megaprime DNA labeling system (Amersham Biosciences).

**Quantitative RT-PCR.** Total cellular RNAs were extracted from the testes of 16-week-old *Tslc1*$^{+/+}$ and *Tslc1*$^{-/-}$ mice using an RNeasy Mini kit (QIAGEN, Valencia, CA). One microgram of total cellular RNA was reverse transcribed using Superscript II reverse transcriptase (RT; Invitrogen) with oligo(dT) primers, and an aliquot was amplified by real-time PCR using a Light Cycler instrument with Master SYBR green I (Roche, Mannheim, Germany). The sequences of the oligonucleotide primers used for PCR are listed in Table S1 in the supplemental material.

**Antibodies.** A rabbit polyclonal antibody against 18 amino acids at the carboxyl termini of human and mouse TSLC1/IGSF4 (CC2) was generated previously

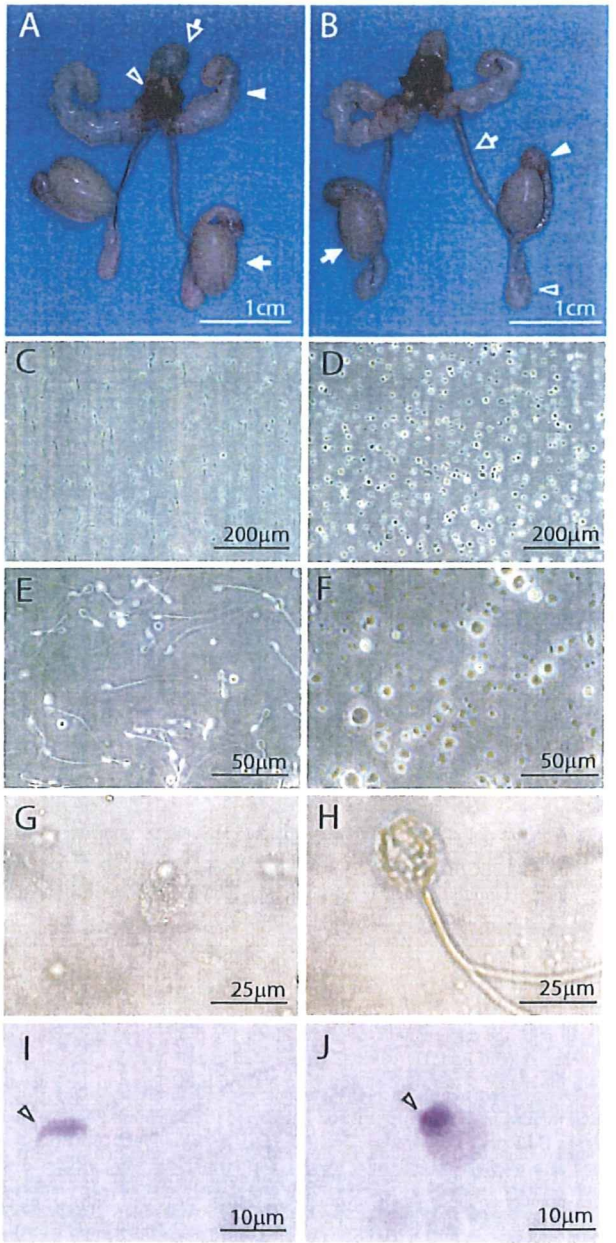


FIG. 2. Reproductive organs and semens from *Tslc1*$^{+/+}$ and *Tslc1*$^{-/-}$ male mice. (A and B) Morphology of reproductive organs from *Tslc1*$^{+/+}$ (A) and *Tslc1*$^{-/-}$ (B) mice. The bladder (open arrow in panel A), prostate (open arrowhead in panel A), seminal vesicles (closed arrowhead in panel A), testes (closed arrow in panels A and B), vasa deferentia (open arrow in B), caput epididymides (closed arrowhead in panel B), and cauda epididymides (open arrowhead in panel B) are demonstrated. Note that the testes from the *Tslc1*$^{-/-}$ mice are significantly smaller than those from the *Tslc1*$^{+/+}$ mice. (C to H) Phase-contrast microscopy of semens from *Tslc1*$^{+/+}$ (C and E) and *Tslc1*$^{-/-}$ (D and F to H) mice. (I and J) PAS staining of semens from *Tslc1*$^{+/+}$ (I) and *Tslc1*$^{-/-}$ mice (J). The open arrowhead indicates a possible acrosome with PAS staining.

TABLE 1. Weights of organs, sperm parameters, and serum testosterone levels in *Tslc1*$^{-/-}$ and *Tslc1*$^{+/+}$ mice

| Parameter | Value for *Tslc1*$^{-/-}$ mice | No. of mice analyzed | Value for *Tslc1*$^{+/+}$ mice | No. of mice analyzed | *P* value[b] |
|---|---|---|---|---|---|
| Total body wt (g) (25 wks) | 38.7 ± 2.8 | 4 | 37.8 ± 1.6 | 4 | NS |
| Wet wt of organs (mg)[a] | | | | | |
| Brain | 425 ± 10 | 3 | 442 ± 7.9 | 4 | NS |
| Eye | 25.5 ± 0.4 | 5 | 24.4 ± 2.1 | 3 | NS |
| Thymus | 38.7 ± 0.9 | 3 | 42.4 ± 2.2 | 3 | NS |
| Lung | 174 ± 28 | 3 | 181 ± 7.2 | 4 | NS |
| Heart | 222 ± 23 | 5 | 189 ± 19 | 4 | NS |
| Spleen | 85.5 ± 19 | 5 | 94 ± 5.0 | 4 | NS |
| Kidney | 318 ± 22 | 5 | 309 ± 22 | 4 | NS |
| Liver | 1,900 ± 80 | 5 | 1,770 ± 260 | 4 | NS |
| Stomach | 420 ± 54 | 4 | 405 ± 54 | 3 | NS |
| Intestinum tenue, pancreas, and mesenterium | 2,310 ± 130 | 5 | 2,470 ± 280 | 4 | NS |
| Intestinum crassum | 584 ± 78 | 3 | 651 ± 47 | 3 | NS |
| Seminal vesicle | 163 ± 14 | 4 | 153 ± 4.2 | 4 | NS |
| Bladder and prostate | 133 ± 18 | 4 | 143 ± 10 | 4 | NS |
| Epididymis and vas deferens | 59.4 ± 9.5 | 5 | 85.1 ± 13 | 4 | NS |
| Testis | 94.7 ± 3.0 | 5 | 134 ± 8.7 | 4 | 0.003 |
| Sperm parameters (11 wks) | | | | | |
| Total no. of cells ($10^6$) | 7.3 ± 1.0 | 3 | 20 ± 2.4 | 3 | 0.008 |
| No. of normal sperm ($10^3$) | 1.2 ± 0.8 | 3 | 15,000 ± 2,200 | 3 | 0.002 |
| Motile sperm/normal sperm (%) | 1.1 ± 0.4 | 3 | 83.3 ± 3.3 | 3 | <0.0001 |
| Serum testosterone level (ng/ml) | | | | | |
| 16 wks | 4.5 ± 4.0 | 3 | 2.5 ± 2.0 | 3 | NS |
| 25 wks | 1.7 ± 0.5 | 4 | 3.2 ± 3.0 | 4 | NS |

[a] Brains and lungs were from 16-week-old mice. Other organs were from 25-week-old mice. For each animal, the wet weights of paired organs were averaged, and this single value was used to calculate the means ± SE.
[b] NS, not significant.

(10). A rabbit polyclonal antibody against the extracellular domains of human and mouse TSLC1/IGSF4 (EC2) was gifted from H. P. Ghosh at McMaster University, Hamilton, Canada. An anti-alpha-tubulin antibody was purchased from Santa Cruz Biotechnology (Santa Cruz, CA).

**Western blotting.** The testes of 25-week-old mice were removed and homogenized in a lysis buffer (1% Triton X-100, 50 mM Tris-HCl, pH 7.4, 150 mM NaCl, 5 mM EDTA, 1× protease inhibitor cocktail set I [Calbiochem, Darmstadt, Germany]) to obtain cell lysates. After centrifugation at 3,000 rpm at 4°C for 10 min, the supernatants were examined for protein concentration using Benchmark (Bio-Rad, Hercules, CA) and used as cell lysates. The cell lysates from the mouse testes were subjected to NuPAGE bis-Tris 4 to 12% gel electrophoresis with a morpholinepropanesulfonic acid-sodium dodecyl sulfate (MOPS-SDS) running buffer (Invitrogen) and transferred to Immobilon-P transfer membranes (Millipore Corporation, Bedford, MA). SeeBlue Plus2 (Invitrogen) was used as a marker for molecular weight. The membranes were incubated with each primary antibody at 4°C overnight and then incubated with horseradish peroxidase-linked secondary antibodies (1:5,000; Amersham Biosciences) at room temperature for 1 h after being washed with Tris-buffered saline containing 0.1% Triton X-100. The membranes were treated with Lumi-Light$^{plus}$ Western blotting substrate (Roche), and the signals were detected with Hyperfilm (Amersham Biosciences). After incubation with a stripping buffer (2% SDS, 62 mM Tris-HCl, pH 6.8, 0.7% beta-mercaptoethanol) at 50°C for 30 min, the membranes were reprobed with other antibodies or stained with Coomassie brilliant blue.

**Deglycosylation.** Digestion of sites of N-linked glycosylation was carried out using peptide *N*-glycosidase F (New England Biolabs, Beverly, MA) according to the manufacturer's instructions. Briefly, 20 μg of protein from cell lysates of the testes in 90 μl lysis buffer was denatured with 10 μl of glycoprotein denaturing buffer (5% SDS, 10% beta-mercaptoethanol) at 100°C for 10 min and then incubated with 10 μl of G7 buffer (0.5 M sodium phosphate, pH 7.5) and 10 μl of 10% NP-40 containing 1,500 U of peptide *N*-glycosidase F at 37°C for 5 h.

**Sperm counts and motility.** After 2- to 21-week-old mice were sacrificed by cervical dislocation, their epididymides and vasa deferentia were immediately removed, cut into 2-mm-long pieces, resuspended in 1 ml of buffer containing 75 mM NaCl, 24 mM EDTA, and 0.4% bovine serum albumin, and then homogenized to dissociate somatic cells at 32°C for 10 min. The sperm cells remaining as a monodispersed suspension were counted on a hemacytometer. The motility of the sperm obtained from the epididymides and vasa deferentia was examined as reported previously (1).

**Morphological examination and immunohistochemistry.** Mice 2 to 40 weeks old were necropsied for histopathological examination. The testes, epididymides, and vasa deferentia were immediately removed and fixed in Bouin's solution. The whole body was perfused with 7.4% formaldehyde solution. All organs and/or tissues were routinely processed, embedded in paraffin, and stained with hematoxylin and eosin (HE). The testes, epididymides, and vasa deferentia from *Tslc1*$^{+/+}$, *Tslc1*$^{+/-}$, and *Tslc1*$^{-/-}$ mice were stained with periodic acid-Schiff stain (PAS) to identify the stage of spermatid development. For immunohistochemistry, serial sections of the testes were heated to 105°C for 5 min with an antigen retrieval buffer (DakoCytomation, Glostrup, Denmark) after deparaffinization and dehydration for antigen retrieval. Nonspecific reactions were blocked with 5% normal donkey serum in phosphate-buffered saline (PBS). All sections were incubated with each primary antibody at 4°C overnight. The sections were then incubated with a horseradish peroxidase-labeled polymer (DakoCytomation) at room temperature for 1 h, rinsed with PBS, and visualized with 3,3′-diaminobenzidine (DakoCytomation). All sections were counterstained with hematoxylin.

**Terminal deoxynucleotidyltransferase-mediated dUTP-biotin nick end labeling (TUNEL) assays.** Testes from 21-week-old mice were fixed with paraformaldehyde and embedded in paraffin. After deparaffinization and dehydration, testicular sections from *Tslc1*$^{+/+}$ mice and *Tslc1*$^{-/-}$ mice (12 sections from 3 mice in each group) were treated with 20 μg/ml proteinase K for 15 min. $H_2O_2$ solution was used for endogenous peroxidase blocking. The sections were incubated at 4°C overnight with terminal deoxynucleotidyl transferase labeling safe buffer (Takara Bio, Kyoto, Japan). After being rinsed with PBS, the sections were incubated with anti-fluorescein isothiocyanate–horseradish peroxidase conjugate (Takara Bio) at 37°C for 1 h, rinsed with PBS, and visualized with 3,3′-diaminobenzidine (DakoCytomation). All sections were counterstained with methyl green (Cab Vision, Fremont, CA).

**Flow cytometry.** Testes were excised from 19-week-old *Tslc1*$^{+/+}$ and *Tslc1*$^{-/-}$ mice (three mice in each group) and decapsulated and crushed through 20-gauge needles and 100-μm cell strainers (BD Falcon, Bedford, MA) in PBS. The cells ($2 \times 10^6$) were then treated with RNase and stained with propidium iodide using a Cycle Test Plus DNA reagent kit (Becton Dickinson, San Jose, CA). All fluorescence-activated cell sorting data were analyzed using CELL Quest (version 3.3; Becton Dickinson).

**Electron microscopy.** *Tslc1*$^{+/+}$ and *Tslc1*$^{-/-}$ mice (25 weeks old) were perfused with 3% glutaraldehyde (Sigma-Aldrich, St. Louis, MO) buffered with

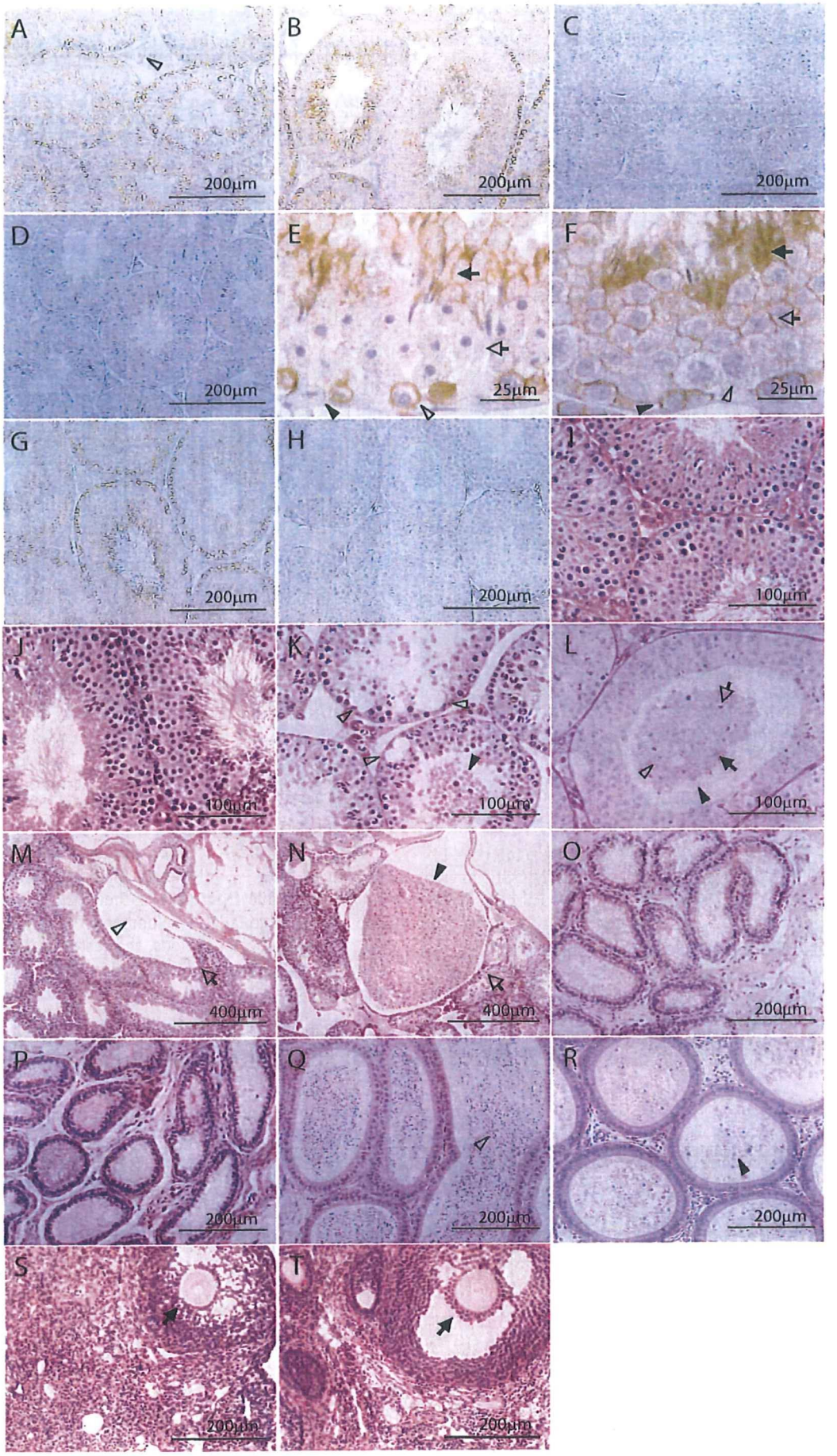
A
200μm
B
200μm
C
200μm
D
200μm
E
25μm
F
25μm
G
200μm
H
200μm
I
100μm
J
100μm
K
100μm
L
100μm
M
400μm
N
400μm
O
200μm
P
200μm
Q
200μm
R
200μm
S
200μm
T
200μm

PBS, pH 7.4, through the heart to fix all organs and tissues. The testes and epididymides were then removed, cut into 1-mm$^3$ pieces, and stored in the same fixative at 4°C for 4 h. After being rinsed with PBS, the tissues were postfixed with 1% osmium tetroxide (Electron Microscopy Sciences, Hatfield, PA) at 4°C for 2 h. Thereafter, the samples were routinely processed, dehydrated with ethanol, and embedded in epoxy resin (TAAB, Berkshire, England). Semithin sections (0.5 μm) of the testes and epididymides were stained with toluidine blue. Ultrathin sections of the selected area were cut on a copper grid, stained with uranyl acetate and lead citrate, and examined by transmission electron microscopy in a JEM-1011 electron microscope (JEOL, Tokyo, Japan).

**Oligonucleotide microarray.** The protocol used for sample preparation and microarray processing is available from Affymetrix (Santa Clara, CA). Briefly, 3 μg purified RNA, extracted from the testes of 16-week-old *Tslc1*$^{+/+}$ and *Tslc1*$^{-/-}$ mice, was reverse transcribed with Superscript II reverse transcriptase (Invitrogen), using primer T7-dT24 containing a T7 RNA polymerase promoter. After a second strand of cDNA was synthesized using RNase H, *Escherichia coli* DNA polymerase, and *E. coli* DNA ligase, in vitro transcription was carried out on the cDNA to produce a biotin-labeled cRNA with a MEGAscript High Yield transcription kit (Ambion, Austin, TX), as recommended by the manufacturer. After the cRNA was linearly amplified with T7 polymerase, the biotinylated cRNA was cleaned with an RNeasy mini column (QIAGEN), fragmented to 50 to 200 nucleotides, and then hybridized to mouse genome U74A v. 2 arrays (Affymetrix). The stained microarrays were scanned with a GeneArray scanner (Affymetrix), and the signals were calculated with the Affymetrix software Microarray Suite 5.0. All of the data were scaled with the global scaling method to adjust the target intensity to 1,000.

**Data analysis.** For microarray analysis, the expression value for each gene was determined by calculating the average difference (perfect match intensity minus mismatch intensity) for the probe in use for the gene. The degree of change was calculated for each sample relative to the median of the controls. Small and negative expression levels were clipped off so that they would be equal to a cutoff value arbitrarily chosen as 100. For all comparisons, statistical analysis was carried out by Student's *t* test, using the Stat View statistical analysis software package (version 5.0; SAS Institute, Cary, NC).

**Microarray accession number.** Microarray data were deposited in the GEO database at NCBI with the accession number GSE3676.

## RESULTS

**Male mice deficient in the *Tslc1/Igsf4* gene were infertile.** For the purpose of exploring the function of TSLC1/IGSF4 in vivo, we inactivated the *Tslc1/Igsf4* gene in mouse ES cells by targeted disruption of exon 1 of the gene, thereby generating *Tslc1/Igsf4*-deficient mice (Fig. 1A). The targeting vector was introduced into ES cell lines, and cells that showed targeted recombination were used for the generation of mice that transmitted the disrupted gene. These mice were then mated to produce *Tslc1*$^{-/-}$ mice. The offspring of *Tslc1*$^{+/-}$ intercrosses were born at the expected Mendelian frequencies. Inheritance of the targeted gene was determined by Southern blotting (Fig. 1B) and monitored by PCR using two pairs of primers (WT2F-SA7R and N1F-SA5R) that flanked the recombination sites (Fig. 1C; see Table S1 in the supplemental material). The Tscl1/Igsf4 transcript was not detected in testes from *Tslc1*$^{-/-}$ mice by RT-PCR (Fig. 1D).

Expression of the TSLC1/IGSF4 protein was examined by Western blotting using an anti-TSLC1/IGSF4 antibody, CC2 (10). An immunoreactive signal of approximately 100 kDa, as well as a weak signal of 70 kDa, was detected in testes from *Tslc1*$^{+/+}$ and *Tslc1*$^{+/-}$ mice, whereas no signals were detected in testes from *Tslc1*$^{-/-}$ mice (Fig. 1E). TSLC1/IGSF4 expression was also absent in other tissues from *Tslc1*$^{-/-}$ mice (data not shown), indicating that TSLC1/IGSF4 was not produced in *Tslc1*$^{-/-}$ mice. TSLC1/IGSF4 is an IgCAM carrying six potential asparagine (N)-linked glycosylation sites in its extracellular loops, and it has been shown to be modified by N glycosylation (10). Therefore, we carried out enzymatic deglycosylation of the TSLC1/IGSF4 protein by treatment with *N*-glycosidase F. As shown in Fig. 1E, a single signal of approximately 60 kDa was observed by Western blotting after *N*-glycosidase F treatment, indicating that the signals of both 100 kDa and 70 kDa were specific to the TSLC1/IGSF4 protein and were generated by distinct posttranslational modifications.

*Tslc1*$^{+/-}$ and *Tslc1*$^{-/-}$ mice did not show any overt developmental abnormalities, although significant amounts of TSLC1/IGSF4 protein were expressed in the brains and lungs, in addition to the testes, of *Tslc1*$^{+/+}$ mice (data not shown). Intercrosses between *Tslc1*$^{-/-}$ mice, however, failed to produce any progeny. Male *Tslc1*$^{-/-}$ mice were infertile, whereas female *Tslc1*$^{-/-}$ mice as well as male and female *Tslc1*$^{+/-}$ mice were fertile.

**Semen from *Tslc1*$^{-/-}$ mice contained degenerated cells.** The growth of *Tslc1*$^{-/-}$ mice from birth to young adulthood was indistinguishable from that of their *Tslc1*$^{+/+}$ littermates, except for male gonadal development. During the fetal, postnatal, and prepubertal periods, the testes of *Tslc1*$^{-/-}$ mice developed without any macroscopic abnormalities and had normal testicular descent. However, the weights of the testes in *Tslc1*$^{-/-}$ mice at 11 and 25 weeks of age were 12% ($P = 0.03$) and 29% ($P = 0.003$) lower than those in the respective *Tslc1*$^{+/+}$ mice (Fig. 2A and B; Table 1). On the other hand,

FIG. 3. Immunohistochemical and histological analyses of *Tslc1*$^{+/+}$, *Tslc1*$^{+/-}$, and *Tslc1*$^{-/-}$ mice. (A to H) Immunohistochemical analysis of TSLC1/IGSF4 protein in testes from *Tslc1*$^{+/+}$ (A and D to G), *Tslc1*$^{+/-}$ (B), and *Tslc1*$^{-/-}$ (C and H) mice, using the anti-TSLC1/IGSF4 antibodies CC2 (A to F) and EC2 (G and H). (A and B) The TSLC1/IGSF4 protein was detected in the seminiferous tubules but not in the interstitial compartment, including the Leydig cells (open arrowhead in panel A). (C) The TSLC1/IGSF4 protein was not detected in a testis from a *Tslc1*$^{-/-}$ mouse. (D) No signals were detected by CC2 preincubated with an excess amount of antigenic polypeptides. (E) Seminiferous epithelium at stage I. The TSLC1/IGSF4 protein was localized along the membranes of step 13 spermatids (closed arrow) and early pachytene spermatocytes (open arrowhead) but was not detected in step 1 spermatids (open arrow) or the Sertoli cells (closed arrowhead). (F) Seminiferous epithelium at stage VII. The TSLC1/IGSF4 protein was localized along the membranes of step 7 spermatids (open arrow), step 16 residual bodies (closed arrow), and preleptotene spermatocytes (closed arrowhead) but was not detected in the late pachytene spermatocytes (open arrowhead). (I to T) Histological analyses of the testes (I to N), ductuli efferentes testis (O and P), epididymides (Q and R), and ovaries (S and T) from *Tslc1*$^{+/+}$ (I, M, O, Q, and S), *Tslc1*$^{+/-}$ (J), and *Tslc1*$^{-/-}$ (K, L, N, P, R, and T) mice by HE staining (I to K and M to T) or PAS staining (L). (K) Degenerated round cells were accumulated in the lumen (closed arrowhead), and extensive vacuolization was observed at the basal side (open arrowheads). (L) A large number of round and degenerated cells were seen in the lumen (closed arrowhead). Note that some of the cells in the lumen were stained with PAS and appeared to be derived from round spermatids (open arrowhead), elongating spermatids (open arrow), or the pachytene spermatocytes (closed arrow). (M to R) The open arrows (M and N), open arrowheads (M and Q), and closed arrowheads (N and R) indicate the rete of the testis, the spermatozoa, and the degenerated round cells, respectively. (S and T) Closed arrows indicate the secondary follicle. Mice were examined at 25 weeks of age (A to R) and 40 weeks of age (S and T).

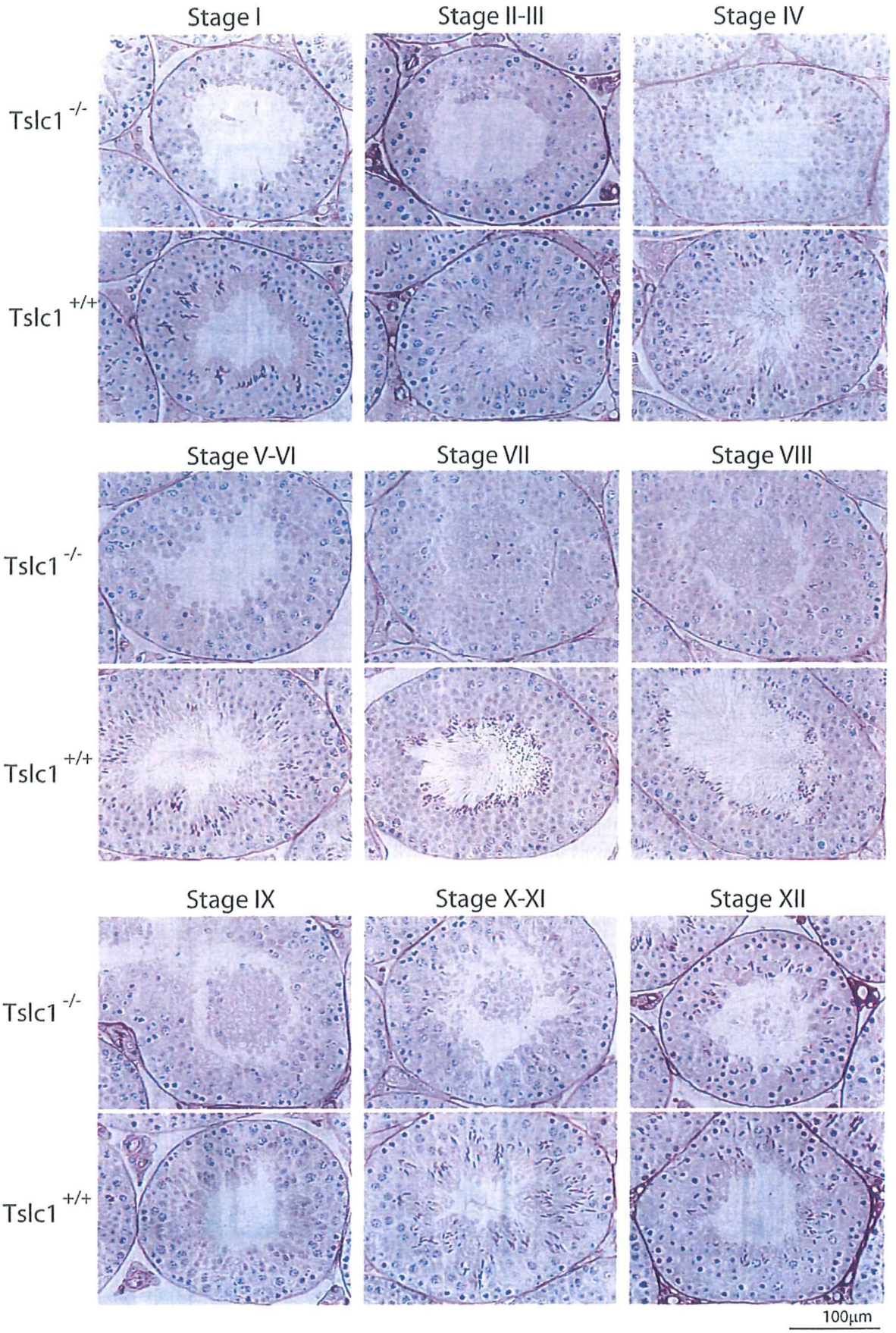


FIG. 4. Staging analyses of the testes from 21-week-old *Tslc1*$^{+/+}$ and *Tslc1*$^{-/-}$ mice by PAS staining.

TABLE 2. Sloughed cells from seminiferous epithelium in testes from *Tslc1*$^{-/-}$ mice[a]

| Type of cells | No. of cells (%) |
|---|---|
| Spermatogonia | 0 (0.0) |
| Spermatocytes | 12 (2.5) |
| Spermatids | 474 (97.5) |
| Steps 1–3 | 16 (3.3) |
| Steps 4–6 | 84 (17.3) |
| Steps 7–9 | 298 (61.3) |
| Steps 10–13 | 38 (7.8) |
| Steps 14–16 | 38 (7.8) |
| Total | 486 (100) |

[a] Twelve testicular sections from three 25-week-old *Tslc1*$^{-/-}$ mice were examined.

there was no significant difference either in the weights of other organs, including the seminal vesicles, epididymides, and vasa deferentia, or in the serum testosterone levels in *Tslc1*$^{-/-}$ mice and *Tslc1*$^{+/+}$ mice (Fig. 2A and B; Table 1).

We then examined semens from the epididymides and vasa deferentia of *Tslc1*$^{-/-}$ mice to determine the mechanisms of male infertility. Phase-contrast microscopy demonstrated that most of the semens from 16-week-old *Tslc1*$^{-/-}$ mice consisted of degenerated, uncharacterized round cells with varied morphologies (Fig. 2D, F, and G), in contrast with those from *Tslc1*$^{+/+}$ mice (Fig. 2C and E). In addition, the number of normal sperm from *Tslc1*$^{-/-}$ mice was approximately 0.01% that from 11-week-old *Tslc1*$^{+/+}$ mice (Table 1). Furthermore, almost all sperm from *Tslc1*$^{-/-}$ mice showed abnormal morphologies, such as large round heads (Fig. 2G), short tails, and multiple tails (Fig. 2H). In addition, the proportion of normal motile sperm in a low-viscosity buffer was only 1.1% for *Tslc1*$^{-/-}$ mice, whereas 83% of the sperm from *Tslc1*$^{+/+}$ mice were highly mobile under the same conditions (Table 1). These findings indicate that male infertility in *Tslc1*$^{-/-}$ mice is due to quantitative and qualitative defects in mature sperm. We next stained uncharacterized round cells in semens from 16-week-old *Tslc1*$^{-/-}$ mice with PAS to detect the acrosome. As shown in Fig. 2J, the perinuclear spaces of the round cells were stained with PAS, suggesting that these cells are derived from immature spermatids.

**Elongated spermatids were scarcely observed in testes from *Tslc1*$^{-/-}$ mice.** Immunohistochemical studies of *Tslc1*$^{+/+}$ and *Tslc1*$^{+/-}$ mice with the CC2 antibody against the carboxyl-terminal end of TSLC1/IGSF4 demonstrated that the TSLC1/IGSF4 protein was present in the seminiferous tubules but not in the interstitial tissues, including the Leydig cells (Fig. 3A and B). On the other hand, no signal of the TSLC1/IGSF4 protein was detected in testes from *Tslc1*$^{-/-}$ mice (Fig. 3C). The signals observed in the testes from *Tslc1*$^{+/+}$ mice disappeared when the CC2 antibody was preincubated with the antigenic polypeptide (Fig. 3D). Detailed analysis of the seminiferous epithelium revealed that the TSLC1/IGSF4 protein was expressed in two distinct phases of spermatogenesis: the first phase was from intermediate spermatogonia to early pachytene spermatocytes, and the second phase was from step 7 to step 16 spermatids (Fig. 3E and F). The TSLC1/IGSF4 protein was located along the membrane in these spermatogenic cells but was not present in the Sertoli cells. We also confirmed a lack of TSLC1 expression in testes from *Tslc1*$^{-/-}$ mice with the EC2 antibody against the extracellular domain of TSLC1 (Fig. 3G and H).

Morphologically normal spermatogenic features were observed in the testes from *Tslc1*$^{+/+}$ and *Tslc1*$^{+/-}$ mice, in which elongating or elongated spermatids were present in the seminiferous epithelia (Fig. 3I and J). In contrast, elongating or elongated spermatids were scarcely observed in seminiferous epithelia from *Tslc1*$^{-/-}$ mice (Fig. 3K and L). Instead, a large number of round cells with degeneration accumulated in the lumens and retia from *Tslc1*$^{-/-}$ mice (Fig. 3K, L, and N, closed arrowheads). Considerable numbers of vacuoles were also specifically observed at the basal area of the seminiferous tubules (Fig. 3K, open arrowheads). On the other hand, the basal lamina, spermatogonia, and interstitial compartments, including Leydig cells, were unaffected in testes from *Tslc1*$^{-/-}$ mice (Fig. 3K). As shown in Fig. 3L, PAS reaction revealed that the cells in the lumen were derived from the round spermatid (open arrowhead), the elongating spermatid (open arrow), or the pachytene spermatocyte (closed arrow). The ductal structure of the ductuli efferentes testis and the epididymides from *Tslc1*$^{-/-}$ mice also showed no abnormalities in comparison

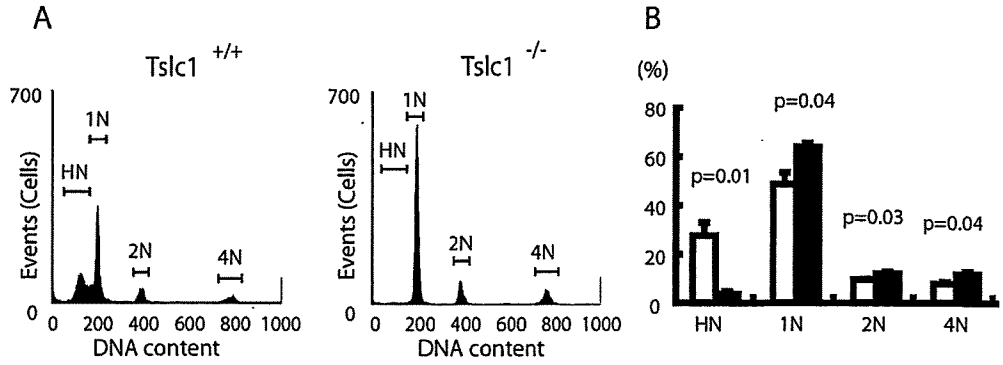


FIG. 5. Flow cytometric analyses of cells isolated from the testes of *Tslc1*$^{+/+}$ and *Tslc1*$^{-/-}$ mice. (A) The flow cytograms demonstrate four discrete peaks: an HN (haploid) peak representing elongated spermatids, a 1N (haploid) peak representing round spermatids, a 2N (diploid) peak representing $G_1$-phase spermatogonia, and a 4N (tetraploid) peak representing pachytene spermatocytes and $G_2$-phase spermatogonia. (B) Relative amounts of four cell populations in the testes. Open and closed boxes indicate cells from *Tslc1*$^{+/+}$ and *Tslc1*$^{-/-}$ mice, respectively.

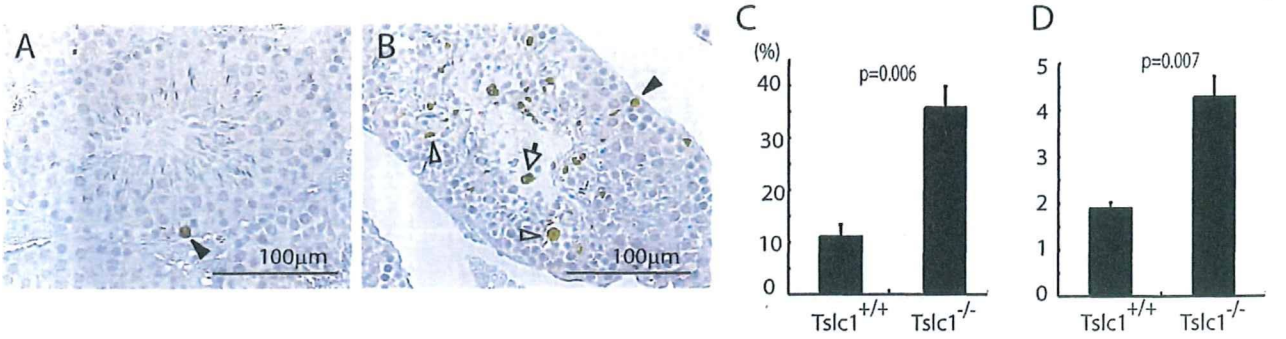


FIG. 6. Detection of apoptosis by TUNEL assays. (A and B) Histochemistry of the testes from *Tslc1*$^{+/+}$ (A) and *Tslc1*$^{-/-}$ (B) mice by TUNEL assay. Cells stained brown are TUNEL-positive cells. Nuclei were counterstained with methyl green (green). Closed arrowheads and open arrowheads indicate spermatocytes and spermatids, respectively. The open arrow indicates the sloughed cell. (C) Ratios of TUNEL-positive tubules to total tubules. (D) Average numbers of TUNEL-positive cells in TUNEL-positive tubules.

with those from *Tslc1*$^{+/+}$ mice (Fig. 3O to R). Since the degenerated round cells were present in the epididymides from *Tslc1*$^{-/-}$ mice (Fig. 3R, closed arrowhead), the seminal tracts did not appear to be obstructed. In contrast to male *Tslc1*$^{-/-}$ mice, male and female *Tslc1*$^{+/-}$ mice and female *Tslc1*$^{-/-}$ mice were fertile. Histological examination of the ovaries showed no significant difference between female *Tslc1*$^{+/+}$ and *Tslc1*$^{-/-}$ mice (Fig. 3S and T).

**Sloughing and apoptosis of spermatids in *Tslc1*$^{-/-}$ mice.** To further characterize the defect in *Tslc1*$^{-/-}$ mice, detailed staging analysis of spermatogenesis was carried out. In *Tslc1*$^{-/-}$ mice, sloughed cells were observed mainly in stages VII to IX (Fig. 4). The numbers of spermatids in steps 10 to 16 were markedly decreased, in contrast to those from *Tslc1*$^{+/+}$ mice. However, synchronous spermatogenesis in each tubule was essentially not affected. To unveil which phase of spermatogenic cells sloughed off into the lumen, we classified the types of sloughed cells and counted the numbers of cells. These analyses characterized only 10 to 15% of the round cells in the lumen, as it was not possible to determine the phases of the remaining cells due to severe degeneration. As shown in Table 2, among the characterized sloughed cells, 98% were determined to be spermatids, and the remaining 2% were spermatocytes in the pachytene phase, while no spermatogonia were observed. Notably, about 60% of the characterized cells were spermatids in steps 7 to 9, suggesting that sloughing from the seminiferous epithelia occurred mainly in the spermatids in steps 7 to 9 in the tubules in stages VII to IX. The absence of spermatids in step 10 and later in the tubules in stages X to XII and I to VIII suggests that the maturation of the majority of the spermatids was arrested around step 10.

We next examined the DNA contents of testicular cells from *Tslc1*$^{+/+}$ and *Tslc1*$^{-/-}$ mice, using flow cytometry (Fig. 5). *Tslc1*$^{-/-}$ mice showed markedly decreased HN cell fractions (representing elongated spermatids [steps 10 to 16]), increased 1N cell fractions (round spermatids [steps 1 to 9]), and slightly increased 2N and 4N cell fractions (spermatogonia and spermatocytes) compared to *Tslc1*$^{+/+}$ mice. This finding is consistent with the histological observation of a maturation arrest of spermatogenesis at the stages between round spermatids and elongated spermatids. In addition, the presence of 1N cell fractions (haploid cells) suggests that meiosis was not affected in *Tslc1*$^{-/-}$ testes.

To examine the possible involvement of apoptosis in the mature arrest of the spermatids, we carried out a TUNEL assay on the testes from *Tslc1*$^{+/+}$ and *Tslc1*$^{-/-}$ mice. A considerable number of spermatocytes and spermatids in *Tslc1*$^{-/-}$ mice were positive in the TUNEL assay (Fig. 6B). In contrast, a small number of spermatocytes, but not spermatids, in *Tslc1*$^{+/+}$ mice were TUNEL positive (Fig. 6A). As shown in Fig. 6C and D, *Tslc1*$^{-/-}$ testes showed significantly increased numbers of TUNEL-positive tubules and TUNEL-positive cells compared with *Tslc1*$^{+/+}$ testes. These results suggest that the primary role of TSLC1/IGSF4 is suppression of apoptosis, although we cannot exclude the possibility that TSLC1/IGSF4 directly functions as a survival factor in sperm development.

**Delayed maturation of spermatocytes in developing *Tslc1*$^{-/-}$ mice.** To understand detailed features of the maturation defect of spermatogenesis in *Tslc1*$^{-/-}$ mice, the postnatal development of the testes was compared in *Tslc1*$^{+/+}$ and *Tslc1*$^{-/-}$ mice (Fig. 7). The spermatogonia and Sertoli cells of 2-week-old mice were observed at the basal sites of the seminiferous tubules. In addition, the primary spermatocytes appeared as round cells with large nuclei at the luminal sites in both *Tslc1*$^{+/+}$ and *Tslc1*$^{-/-}$ mice. The round spermatids appeared at the luminal sites in *Tslc1*$^{+/+}$ mice by 3 weeks of age. In *Tslc1*$^{-/-}$ mice, however, the round spermatids were not seen until 4 weeks of age. Furthermore, elongated spermatids were scarcely observed at all time points in *Tslc1*$^{-/-}$ mice. Therefore, it is speculated that germ cell differentiation is delayed when the spermatocytes proceed to round spermatids and is finally arrested when the round spermatids proceed to elongated spermatids in *Tslc1*$^{-/-}$ mice. In *Tslc1*$^{+/+}$ mice, elongated spermatids and spermatozoa appeared at 4 weeks and 5 weeks of age, respectively. The epididymides from *Tslc1*$^{+/+}$ mice were filled with spermatozoa by 6 weeks of age. In contrast, the round spermatids began to slough into the lumen and multinucleated giant cells appeared at 5 weeks of age in *Tslc1*$^{-/-}$ mice. Sloughing of the spermatids was also seen in mice 5 weeks of age or older. Consistent with these findings, the epididymides were filled with degenerated round cells by the time the mice were 6 weeks of age. Then, several weeks after the

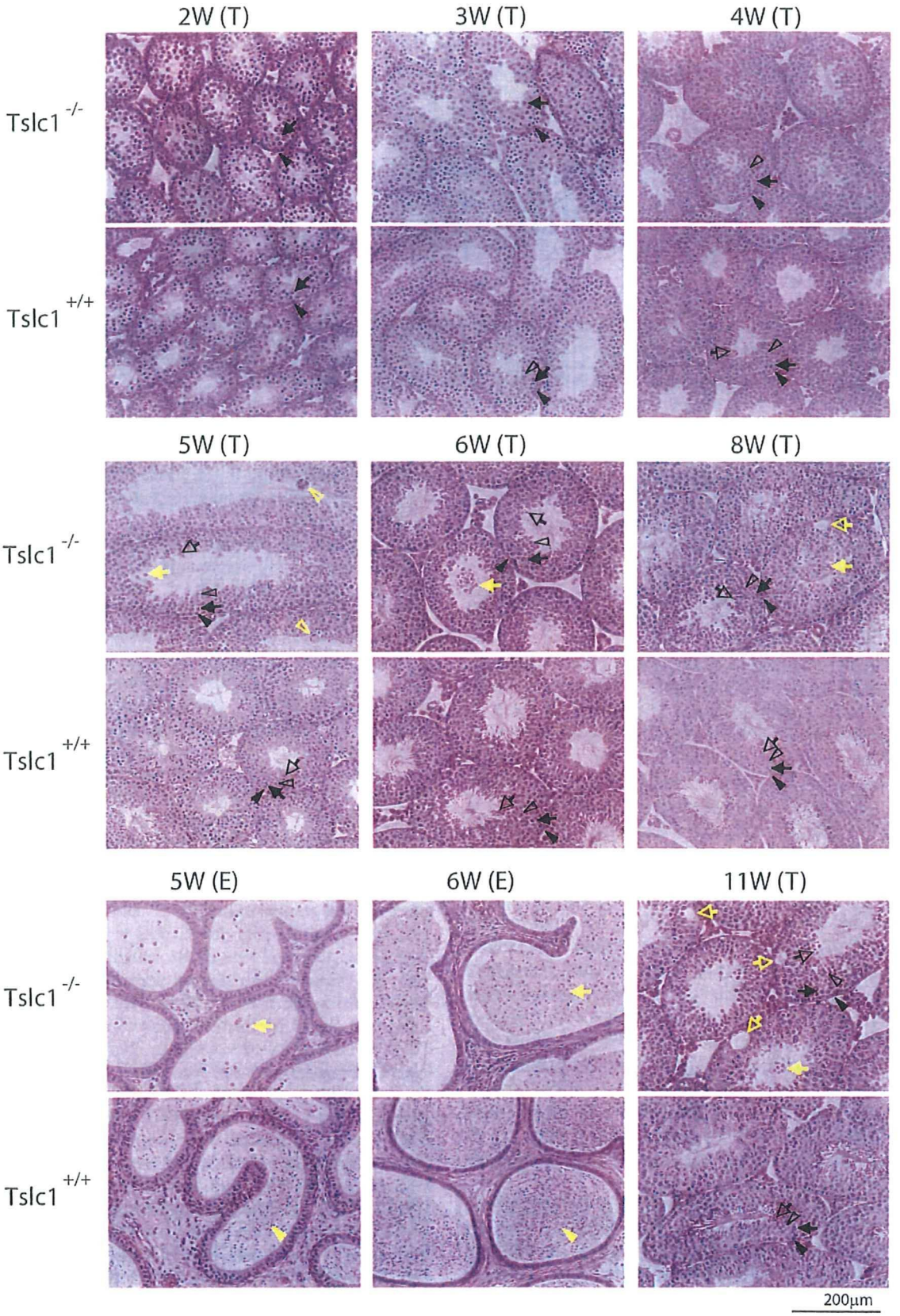


FIG. 7. Morphological analysis of germ cells from *Tslc1*$^{+/+}$ and *Tslc1*$^{-/-}$ mice during postnatal development. Testes (T) and epididymides (E) of juvenile mice from 2 to 11 weeks of age were examined by HE staining. Closed arrowheads, closed arrows, open arrowheads, and open arrows in black indicate spermatogonia, spermatocytes, round spermatids, and elongated spermatids, respectively. Closed arrowheads, closed arrows, open arrowheads, and open arrows in yellow indicate spermatozoa, sloughed cells, multinucleated giant cells, and vacuoles, respectively.